NATIONAL ADVISORY COMMITTEE FOR AERONAUTICS

TECHNICAL NOTE 3985

PROPELLANT VAPORIZATION AS A CRITERION FOR ROCKET ENGINE DESIGN; CALCULATIONS OF CHAMBER LENGTH TO VAPORIZE A SINGLE n-HEPTANE DROP

By Richard J. Priem

Lewis Flight Propulsion Laboratory
Cleveland, Ohio

Washington
July 1957

NATIONAL ADVISORY COMMITTEE FOR AERONAUTICS

TECHNICAL NOTE 3985

PROPELLANT VAPORIZATION AS A CRITERION FOR ROCKET ENGINE DESIGN; CALCULATIONS OF CHAMBER LENGTH TO VAPORIZE A SINGLE n-HEPTANE DROP

By Richard J. Priem

SUMMARY

Calculations based on droplet-evaporation theory show that for a given combustor length the percent of fuel mass vaporized can be increased by decreasing the fuel-drop size and the initial drop velocity, or by increasing chamber pressure, final gas velocity, and initial fuel temperature. The analytical results of this study were correlated to give a single curve of percent of fuel evaporated as a function of the chamber length and the factors involving these parameters. The calculated results agree with experimental results if the mass-mean-drop diameters for various injectors are assumed to be about 100 to 200 microns.

INTRODUCTION

The large number of different phenomena that can have a fundamental role in the combustion within a rocket engine makes it difficult to determine and study the controlling processes. Some of these phenomena, as given in references 1 and 2, are atomization, heating, vaporization, liquid and gaseous diffusion, combustion of droplets, and liquid- or gas-phase reaction. Several papers (refs. 1 to 4) have presented the current concepts used in designing rocket engines and the similarity parameters used in scaling.

These current approaches have been based on flow and chemical-reaction theories. The significance of vaporization was neglected or, at best, included in the analysis by a single dimensionless group. To demonstrate the importance of vaporization, a model was used which assumed that vaporization of the least volatile propellant was the rate-controlling step in rocket-engine combustion. Calculations were made to determine the vaporization rate and also a history of the fuel vaporized as a function of the chamber length. Many engine parameters were varied to

show how such parameters affected the chamber length required to vaporize a given percentage of the least volatile propellant.

Of the various techniques (refs. 5 to 8) for determining vaporization rates, that given in reference 8 seemed most applicable to the conditions encountered in rocket engines. This technique of reference 8 included considerations of the heating-up period of the drop, unidirectional diffusion, and the effect of mass transfer on heat transfer. Furthermore, the results of the technique are in good agreement with the experimental results of single-drop investigations over a wide range of conditions that approach those encountered in rocket engines (refs. 9 to 10). The results were compared with experimental data to determine whether the calculated and experimental results agree.

THEORY

The calculation technique used herein was based on applying known steady-state mass, momentum, and heat-transfer equations to a droplet vaporizing in a rocket engine. The process was divided into small increments during which only small changes occur, as shown by the model of figure 1.

A liquid droplet is shown at position x and a small increment later in time $\Delta\theta$ and distance Δx. During this increment, the drop velocity v changes by a small amount Δv. In this same increment, the gas velocity u changes by Δu. The drop velocity would start at the injection velocity and either slow down or speed up as determined by the drag on the drop. Similarly, the gas velocity starts at zero and increases as the propellants vaporize and burn. While the drop is moving through the increment, heat is transferred to the liquid surface at a constant rate q_v, and fuel is being transferred from the surface at a constant rate w; an oxidant is added to burn the vaporizing fuel instantaneously at stoichiometric conditions. During the increment, the mass and the radius of the drop change from m_1 to m_2 and r_1 to r_2, respectively, while the temperature T_l changes by ΔT_l.

The equations used to determine the mass-transfer rate are as follows:

$$w = AKp_l\alpha \tag{1}$$

$$Nu_M = \frac{2rK}{DM/R\overline{T}} = 2 + 0.6\ Sc^{1/3}Re^{1/2} \tag{2}$$

$$\alpha = \frac{P}{p_l} \ln \frac{P}{P - p_l} \tag{3}$$

A rigorous derivation of equation (1) is given in references 8 and 10. The mass transfer is dependent on (1) the surface area of the drop A, (2) the driving force (vapor pressure of the fuel) p_l, (3) the coefficient of mass transfer K determined by the empirical equation given in reference 11 (eq. (2)), and (4) a factor α as given by equation (3) to correct for unidirectional mass transfer.

The rate of heat transfer to the liquid surface is obtained from the following equations:

$$q_v = Ah(T - T_l)Z \tag{4}$$

$$Nu_h = \frac{h\ 2r}{k_m} = 2 + 0.6\ Pr^{1/3}Re^{1/2} \tag{5}$$

$$Z = \frac{z}{e^z - 1} \tag{6}$$

where

$$z = \frac{wc_{p,f}}{hA}$$

A rigorous derivation of equation (3) is also given in references 8 and 10. The heat transfer is dependent on (1) the surface area A, (2) the driving force $(T - T_l)$, (3) the heat-transfer coefficient h determined from equation (5) as given in reference 11, and (4) a correction factor Z for the heat carried back by the vaporizing fuel.

The heat-transfer rate to the liquid surface q_v is divided into a sensible-heat rate q_L and a vaporization rate to give the following equation:

$$q_v = q_L + w\lambda \tag{7}$$

The change in drop temperature is determined by

$$q_L = m_l c_{p,l} \frac{dT}{d\theta} \tag{8}$$

where m_l is the mass of the drop, $c_{p,l}$ is the specific heat, and $dT/d\theta$ is the rate at which the temperature of the drop increases. A complete list of the symbols used in this report are defined in appendix A.

A change in drop velocity is produced by aerodynamic drag as the drop moves through the gas. For a spherical droplet

$$m \frac{dv}{d\theta} = - C_D A \rho_m \frac{U^2}{2} \tag{9}$$

or

$$\frac{dv}{d\theta} = - \frac{3}{8} C_D \frac{\rho_m U^2}{\rho_l r} \tag{10}$$

The change in drop velocity is dependent on the drag coefficient C_D obtained from reference 12 as

$$C_D = 27 \, Re^{-0.84} \tag{11}$$

The velocity change is, therefore, a function of the mass of the drop m, its area A, the density of the gas ρ_m, and the velocity difference between the gas and the drop U.

The increase in gas velocity is obtained from the following equation, which is derived in appendix B:

$$\frac{du}{d\theta} = - \frac{u_{fin}}{m_0} w \tag{12}$$

The change in gas velocity depends on the ratio of the mass-transfer rate to the initial mass of the drop m_0 and the final gas velocity u_{fin}.

The preceding equations were solved by an iterative procedure on an electronic computer. A linear interpolation was used to obtain average values. A similar procedure was used in references 8 and 10 for other environmental conditions. The boundary conditions that were varied are shown in table I. Physical properties were determined from the equations given in references 9 and 10 for n-heptane. Physical properties other than those of n-heptane were not considered in this analysis.

RESULTS

The results of the calculations are droplet histories, examples of which are shown in figure 2. Droplet temperature, radius, percentage of mass vaporized, drop velocity, gas velocity, and vaporization rate are shown at various positions in the chamber. The calculated temperature

of the droplet rises rapidly to 880° R (corresponding vapor pressure of approximately 180 lb/sq in.), which is the "wet bulb" temperature for the fuel at the conditions specified. The temperature of 880° R agrees with the measured wall temperatures of internal-film coolants. If the correction factor for unidirectional diffusion α, and the effect of mass transfer on heat transfer Z were omitted in the calculation, the temperature would be much higher (usually taken as the temperature for a vapor pressure of 300 lb/sq in.).

4371

The percent-mass-vaporized curve (fig. 2(a)) initially has a very small slope because of the low liquid temperature of the drop. As the drop heats, the slope of the percent-mass-vaporized curve increases. At the end of the drop lifetime, the slope again decreases because of the decrease in drop surface area and because the drop is moving faster as will be described later.

The radius of the drop initially increases and then decreases (fig. 2(a)). The initial increase is produced by thermal expansion of the drop as it heats. After the "wet bulb" temperature is reached, the radius curve is proportional to the cube root of the mass curve.

The gas-velocity curve (fig. 2(b)) is proportional to the percent-mass-vaporized curve as specified by equation (12). Initially, the curve has a small slope, which increases as the drop heats. Near the end of the drop lifetime, the slope again decreases because of the decrease in drop surface area.

The drop velocity first decreases because of the drag produced by the low gas velocity. A minimum is reached when the gas velocity equals the drop velocity. After the minimum point the drop velocity increases because of the drag produced by the high gas velocity.

The curve (fig. 2(b)) showing the vaporization rate per unit length has two peak points and a minimum point. The minimum point occurs when the gas velocity and drop velocity are equal, producing a Reynolds number of zero and a small Nusselt number. The vaporization-rate curve is initially low because the temperature of the fuel is low. At the end of the chamber, the rate is also low because of the small surface of the drop and the high drop velocity.

Curves similar to those of figure 2 were obtained for various conditions. For simplicity in presenting the results, the effects of various conditions will be shown by the percent-mass-vaporized curve and the vaporization-rate curve. Since the 90- to 100-percent vaporized region is important in rocket-engine design, a plot of the percentage of mass unvaporized is also included for better resolution in this region.

Drop Size

The effect of a change in initial drop size from 0.002- (50 microns) to 0.012- (300 microns) inch diameter is shown in figure 3. As expected, the curves show that small drops will vaporize in a shorter chamber. The percent-mass-vaporized and -unvaporized curves have the same shape for all sizes. The vaporization-rate curves all have the same shape; however, they are shifted upwards and to the left for small drops.

Initial-Drop Velocity

Changes produced by varying the initial-drop velocity are shown in figure 4. The percent-mass-vaporized curve (fig. 4(a)) shows that the inflection point, which occurs when the droplet velocity is the same as the gas velocity, varied with initial velocity. The higher the initial velocity, the more mass that is vaporized before the inflection point is reached. The percent-mass-unvaporized curve (fig. 4(b)) shows that a given percent vaporized is obtained in a shorter chamber length for a low initial velocity than with a high velocity. The slopes of the curves vary somewhat with initial velocity but to a reasonable degree of accuracy remain constant with initial velocity. The vaporization-rate curve (fig. 4(c)) shows that the maximum point decreases with higher initial velocities.

Final Gas Velocity

The final gas velocity is defined as the velocity the gases attain when all the propellants are completely burned. The final gas velocity is a function of the ratio of the chamber area to the throat area (contraction ratio). It would correspond to the velocity in the rocket combustion chamber prior to the convergent section of the nozzle if the engine were operating at 100-percent efficiency. The percent-mass-vaporized curve (fig. 5(a)) shows that in the extremely low percent-mass-vaporized region there is little variation in the percent vaporized in a given chamber length with gas velocity. Near the 10-percent mass-vaporized region, a low gas velocity has more mass vaporized in a given chamber length than a high gas velocity. As with initial drop velocity, the inflection point varies with gas velocity. After the inflection point there is a crossover in the curves, and a given percent vaporized is reached in a shorter chamber length with a high gas velocity.

The percent-mass-unvaporized curves (fig. 5(b)) show that all the curves are similar on this plot with the higher gas velocities producing a given percent vaporized in a shorter chamber. Since the final gas velocity is inversely proportional to the contraction ratio, the lower the

contraction ratio, the shorter the chamber required to vaporize a given percent of the fuel. The curves have slightly different slopes for different gas velocities.

The vaporization-rate curve of figure 5(c) shows that the first peak in the curve increases with decreasing gas velocity, and the second peak decreases with decreasing gas velocity. The positions of the peaks are also changed.

Chamber Pressure

The percent-mass-vaporized plot of figure 6(a) shows that a given percent vaporized is obtained in a shorter length with a higher chamber pressure. The percent-mass-unvaporized curve of figure 6(b) also shows that a given percent of mass-unvaporized is obtained in a shorter length with a higher chamber pressure. The slopes of the curves decrease with low chamber pressure. The peaks of the vaporization-rate curves (fig. 6(c)) decrease with increasing chamber pressure and occur at a greater distance from the injector.

Initial Liquid Temperature

Histories for three initial drop temperatures are shown in figure 7. All the curves show that a higher initial liquid temperature is beneficial. The biggest effect is in the very low percent-mass-vaporized region. The vaporization-rate curves are shifted to shorter lengths for higher initial temperature.

Gas Temperature

Histories for gas temperatures of 4000°, 5000°, and 7000° R are shown in figure 8. Except for the time when the drop is heating there is little difference in all the curves as they agree within 10 percent over this extreme temperature condition. For this reason the 5000° R gas temperature used in most of the calculations does not materially affect the applicability of the results.

Correlation of Results

The performance curves were combined to obtain a single curve representing all the results. The multiplication factor on length that would produce the best agreement was obtained from a cross plot of the length required to vaporize 90 percent of the mass. The correlated results obtained from this analysis are shown in figure 9. The spread of

the length in the percent-mass-vaporized curve (fig. 9(a)) was much greater than the spread in the percent-mass-unvaporized curve (fig. 9(b)). The variation in the position of the inflection point produced most of the spread.

The correlated results show that multiplying the chamber length by

$$\frac{p^{0.55}\, u_{fin}^{0.25}\, T_{l,0}^{0.25}}{r_0^{1.45}\, v_0^{0.75}}$$

gives almost a single curve of percent of mass unvaporized as a function of chamber length.

A comparison of experimental data and the correlation curve is shown in figure 10(a). Three different injector types are shown, and the assumed drop size used for each injector is listed. The experimental results agree very well with the generalized results except at the high percent evaporated and percent performance level.

DISCUSSION OF RESULTS

The calculations show that the vaporization process requires considerable chamber length before it is complete. The results indicate that with drops of approximately 200 microns in diameter a chamber length of 8 inches is required to vaporize 90 percent of the mass. This is about the mass mean size of the droplets obtained with many injectors and the length of some rocket chambers. It therefore seems evident that droplet vaporization cannot be neglected in a theory which predicts how to scale engines. In fact, from the results obtained in this investigation it appears that the droplet-vaporization theory can be used in designing rocket engines.

A limitation to the results presented herein occurs because only a single drop is considered to represent all the drops in a rocket chamber. Actually, there must be a distribution of size, with some large and some small drops. This size variation means an addition of numerous histories for various-size drops. The drop distribution will alter the shape of the curves presented herein. The percent-mass-unvaporized curves would be flatter, for example, as shown by the experimental points in figure 10(b), because originally the small drops would vaporize faster than the mean considered, but towards the end of the chamber there would be numerous larger drops, which would weight the curves toward the large-drop curve. Consequently, it is impossible to predict accurately the percent vaporized in a given chamber length of an actual engine. However, since the curves are being added together, the correction factors should be equally

adaptable when there is a drop distribution. Therefore, the correction factors can be used to scale engines and can show qualitatively what changes in the engine are beneficial. Additional calculations are needed when drop-size distribution and spreading are included in the correlation to predict engine performance accurately. The calculations should also be performed for propellants with different physical properties.

SUMMARY OF RESULTS

Calculations were made for n-heptane drops using various drop sizes, injection velocities, final gas velocities, initial fuel temperatures, and chamber pressures to show how these variables would affect the vaporization rate and the chamber lengths required to vaporize the drops. The results are correlated for ease in using them for design purposes.

The calculations have quantitatively shown the following results:

1. The chamber length required for a given percent of fuel vaporized increases with larger drop sizes and higher injection velocity.

2. Chamber lengths required for a given percent vaporized decrease with higher final gas velocity, higher chamber pressures, and higher initial temperatures.

3. Calculated results agree with experimental results when an assumed drop diameter of 100 to 250 microns is used for the experimental results.

4. Results were correlated to a reasonable degree of accuracy for application in engine design.

Lewis Flight Propulsion Laboratory
National Advisory Committee for Aeronautics
Cleveland, Ohio, March 19, 1957

APPENDIX A

SYMBOLS

A	surface area of drop, sq in.
C_D	coefficient of drag for spheres, dimensionless
c_p	specific heat, Btu/(lb)(°F)
D	diffusion coefficient, sq in./sec
h	heat-transfer coefficient, Btu/(sq in.)(sec)(°F)
K	coefficient of mass transfer, sec^{-1}
k	thermal conductivity, Btu/(in.)(sec)(°F)
M	molecular weight of fuel, lb/mole
m	mass of drop, lb
m_x	mass of liquid drop at position x, lb
Nu_h	Nusselt number for heat transfer, dimensionless
Nu_M	Nusselt number for mass transfer, dimensionless
o/f	oxidant to fuel weight ratio, lb/lb
P	total pressure in chamber, lb/sq in.
p_l	vapor pressure of liquid fuel, lb/sq in.
Pr	Prandtl number, $c_{p,m}\mu_m/k_m$, dimensionless
q_L	sensible heating rate of drop, Btu/sec
q_v	heat-transfer rate to surface of drop, Btu/sec
R	universal gas constant, lb/(mole)(°F)
Re	Reynolds number, $2r_0U\rho_m/\mu_m$
r	radius of drop, in.

S	cross-sectional area of chamber, sq in.
Sc	Schmidt number, $\mu_m/D\rho_m$, dimensionless
T	temperature of gas, ^{o}R
$\overline{T}$	mean gas temperature, ^{o}R
T_l	temperature of liquid fuel, ^{o}R
U	velocity difference between gas and drop, in./sec
u	velocity of gas in chamber, in./sec
u_{fin}	final velocity of gas, in./sec
v	droplet velocity, in./sec
w	vaporization rate of fuel, lb/sec
x	axial position of chamber, in.
Z	correction factor for heat transfer, dimensionless
z	heat-transfer factor, dimensionless
α	correction factor for mass transfer, dimensionless
θ	time, sec
λ	latent heat of vaporization, Btu/lb
μ_m	viscosity of vapor mixture, lb/(in.)(sec)
ρ	density, lb/cu in.
$\dot{\omega}$	mass-flow rate, lb/sec
$\dot{\omega}_{ox}$	mass-flow rate of oxidant, lb/sec

Subscripts:

f	fuel vapor
l	liquid fuel

m	vapor mixture
0	beginning of time (run)
1	beginning of increment
2	end of increment

APPENDIX B

DERIVATION OF EQUATION FOR DETERMINING GAS VELOCITY

The gas velocity is obtained by applying a mass balance to the gaseous flow, or

$$\rho_m S\, du = d\dot{\omega}_f + d\dot{\omega}_{ox} \tag{B1}$$

where

ρ_m density of gas

S cross-sectional area of chamber

du change in gas velocity

$d\dot{\omega}_f$ change in mass-flow rate of liquid fuel to vapor

$d\dot{\omega}_{ox}$ change in mass-flow rate of gaseous oxygen

The ratio of oxygen to fuel-flow rate is

$$\frac{\dot{\omega}_{ox}}{\dot{\omega}_f} = o/f \tag{B2}$$

and, therefore,

$$d\dot{\omega}_f + d\dot{\omega}_{ox} = (1 + o/f)\, d\dot{\omega}_f \tag{B3}$$

The following equation results from combining equations (B3) and (B1):

$$du = \frac{(1 + o/f)}{\rho_m S}\, d\dot{\omega}_f \tag{B4}$$

Integrating between the boundary conditions of $u = 0$ and $\dot{\omega}_f = \dot{\omega}_{f,o}$ to $u = u_{fin}$ and $\dot{\omega}_f = 0$ results in

$$u_{fin} = -\frac{(1 + o/f)}{\rho_m S}\, \dot{\omega}_{f,o} \tag{B5}$$

If equations (B5) and (B4) are combined,

$$\frac{du}{u_{fin}} = -\frac{d\dot{\omega}_f}{\dot{\omega}_{f,o}} \tag{B6}$$

The mass-flow rate of fuel can be expressed in terms of the mass of the liquid drop by

$$\dot{\omega}_f = \frac{1}{\tau} m_x \tag{B7}$$

where

m_x mass of the liquid drop at position "x"

τ average time between drops that pass through a cross section of the chamber at a given position (constant throughout the chamber)

The differentiation of equation (B7) gives

$$d\dot{\omega}_f = \frac{1}{\tau} dm_x \tag{B8}$$

The boundary condition $\dot{\omega}_f = \dot{\omega}_{f,0}$ is applied where $m_x = m_0$ so that equation (B7) becomes

$$\dot{\omega}_{f,0} = \frac{1}{\tau} m_0 \tag{B9}$$

A combination of equations (B6), (B8), and (B9) gives the following equation:

$$\frac{du}{u_{fin}} = - \frac{dm_x}{m_0} \tag{B10}$$

and by definition

$$dm_x = w \, d\theta \tag{B11}$$

Therefore,

$$\frac{du}{u_{fin}} = - \frac{w}{m_0} d\theta \tag{B12}$$

REFERENCES

1. Ross, Chandler C.: Scaling of Liquid Fuel Rocket Combustion Chambers. AGARD Selected Combustion Problems, II. Butterworths Sci. Pub., 1956, pp. 444-456.

2. Crocco, L.: Considerations on the Problem of Scaling Rocket Motors. AGARD Selected Combustion Problems, II. Butterworths Sci. Pub., 1956, pp. 457-468.

3. Penner, S. S.: Rational Scaling Procedures for Liquid-Fuel Rocket Engines. Jet Prop., vol. 27, no. 2, pt. 1, Feb. 1957, pp. 156-161.

4. Penner, S. S., and Datner, P. P.: Combustion in Liquid-Fuel Rocket Engines. Fifth Symposium (International) on Combustion, Reinhold Pub. Corp., 1955, pp. 11-29.

5. Godsave, G. A. E.: Studies of the Combustion of Drops in a Fuel Spray - The Burning on Single Drops of Fuel. Fourth Symposium (International) on Combustion, The Williams & Wilkins Co., 1953, pp. 818-830.

6. Ingebo, Robert D.: Vaporization Rates and Heat-Transfer Coefficients for Pure Liquid Drops. NACA TN 2368, 1951.

7. Penner, S. S.: On Maximum Evaporation Rates of Liquid Droplets in a Rocket Motor. Jour. Am. Rocket Soc., vol. 23, no. 2, Mar.-Apr. 1953, pp. 85-88; 98.

8. El Wakil, M. M., Uyehara, O. A., and Myers, P. S.: A Theoretical Investigation of the Heating-Up Period of Injected Fuel Droplets Vaporizing in Air. NACA TN 3179, 1954.

9. El Wakil, M. M., Priem, R. J., Brikowski, H. J., Myers, P. S., and Uyehara, O. A.: Experimental and Calculated Temperature and Mass Histories of Vaporizing Fuel Drops. NACA TN 3490, 1956.

10. Priem, Richard Jerome: Vaporization of Fuel Drops Including the Heating-Up Period. Ph.D. Thesis, Univ. Wis., 1955.

11. Ranz, W. E., and Marshall, W. R., Jr.: Evaporation from Drops. Chem. Eng. Prog., vol. 48, no. 3, Mar. 1952, pp. 141-146.

12. Ingebo, Robert D.: Drag Coefficients for Droplets and Solid Spheres in Clouds Accelerating in Airstreams. NACA TN 3762, 1956.

TABLE I. - BOUNDARY CONDITIONS USED IN CALCULATION

FOR n-HEPTANE

Drop diameter, in.	Final gas velocity, ft/sec	Initial drop velocity, ft/sec	Initial drop temperature, °R	Chamber pressure, lb/sq in.	Gas temperature, °R
0.002	800	100	500	300	5000
.004	↓	↓	↓	↓	↓
.006	↓	↓	↓	↓	↓
.009	↓	↓	↓	↓	↓
.012	↓	↓	↓	↓	↓
.006	↓	50	↓	↓	↓
↓	↓	75	↓	↓	↓
↓	↓	150	↓	↓	↓
↓	↓	200	↓	↓	↓
↓	200	100	↓	↓	↓
↓	400	↓	↓	↓	↓
↓	1200	↓	↓	↓	↓
↓	1600	↓	↓	↓	↓
↓	800	↓	↓	150	↓
↓	↓	↓	↓	600	↓
↓	↓	↓	400	300	↓
↓	↓	↓	700	↓	↓
↓	↓	↓	500	↓	4000
↓	↓	↓	↓	↓	7000
↓	200	50	↓	↓	5000
↓	200	200	↓	↓	↓
↓	1600	200	↓	↓	↓
↓	1600	50	↓	↓	↓

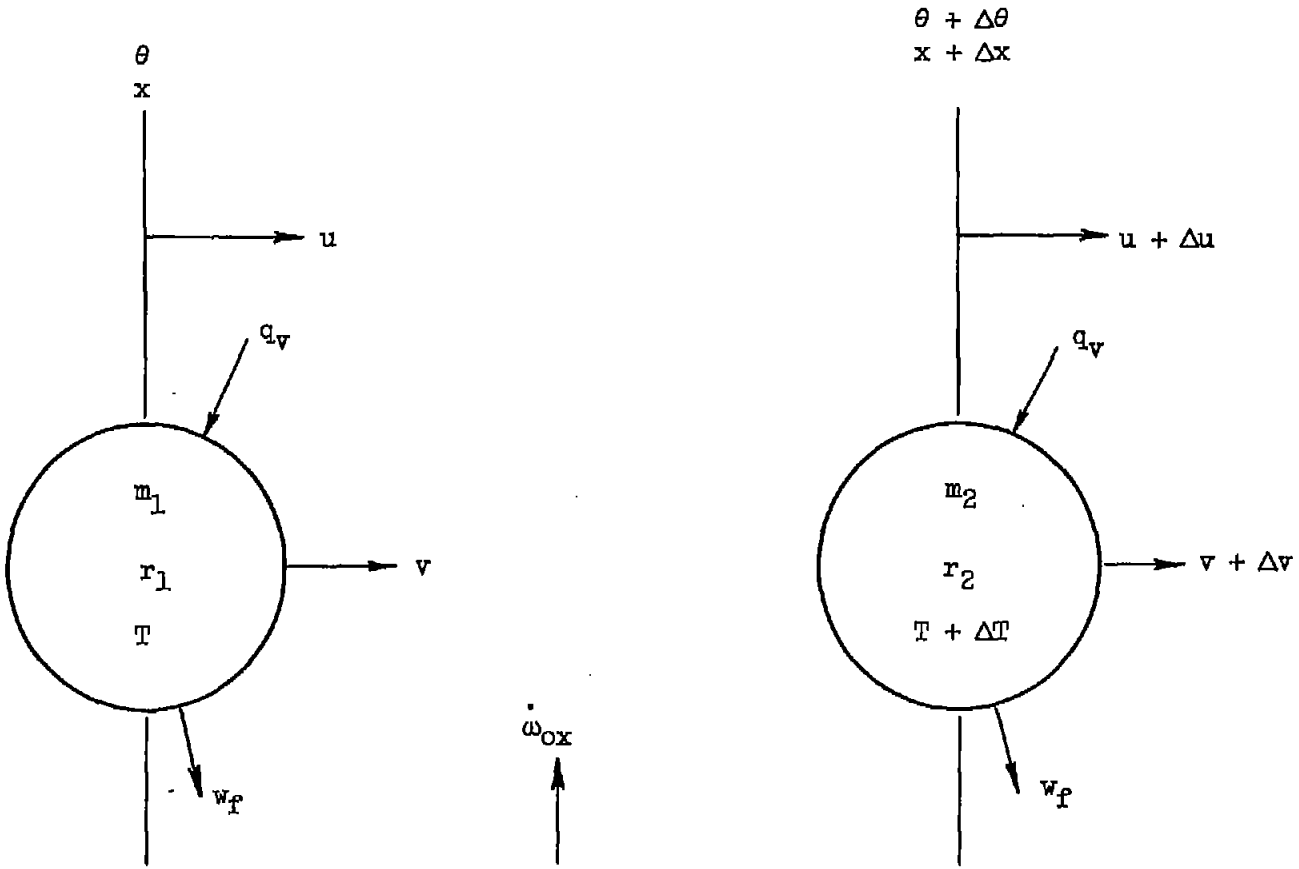

Figure 1. - Schematic drawing of drop vaporizing in rocket engine.

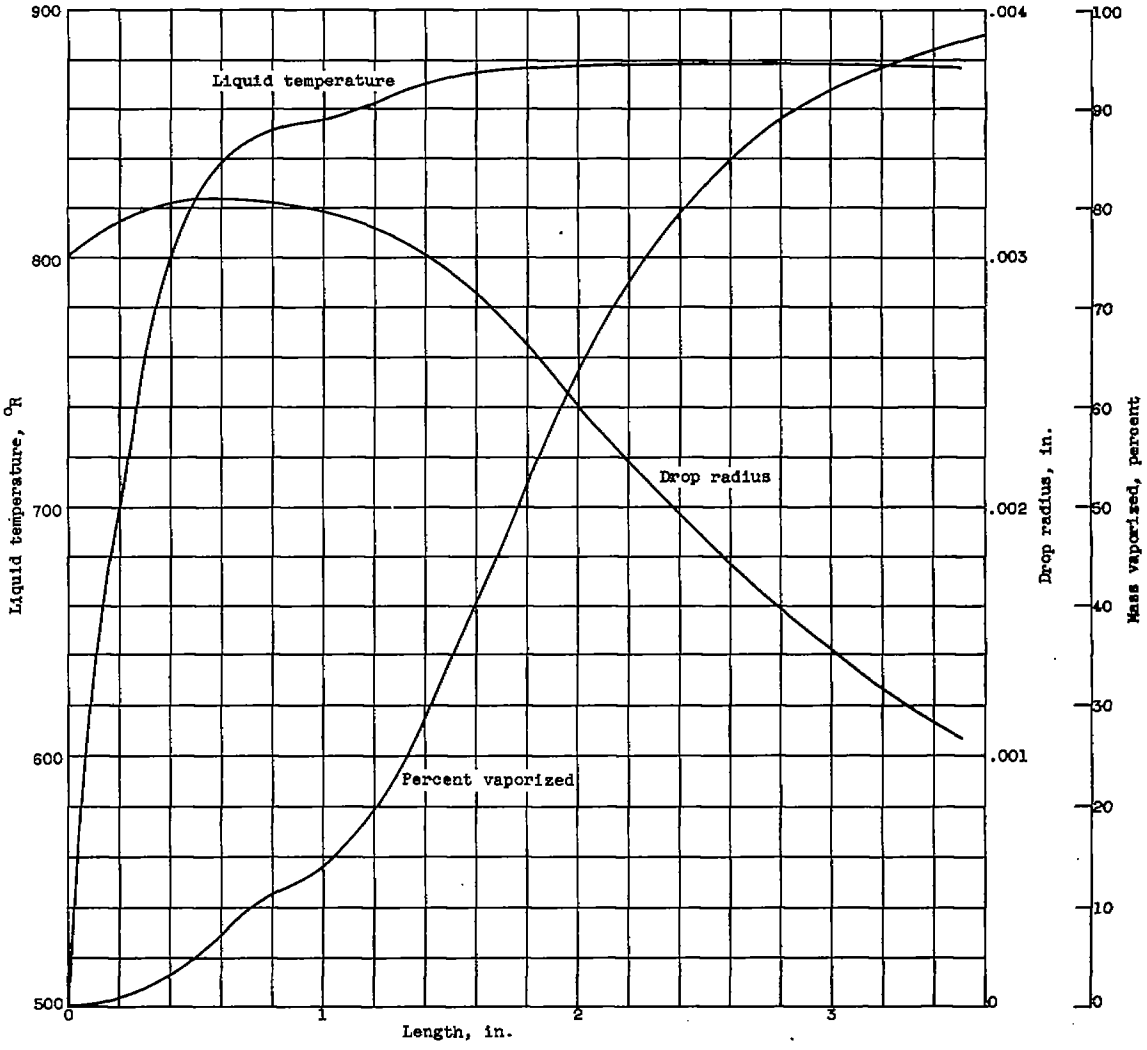

(a) Mass vaporized, drop radius, and liquid temperature.

Figure 2. - Typical droplet histories. Initial drop temperature, 500° R; initial drop velocity, 1200 inches per second; initial drop diameter, 0.006 inch (150 microns); final gas velocity, 9600 inches per second; chamber pressure, 300 pounds per square inch absolute; and chamber temperature, 5000° R.

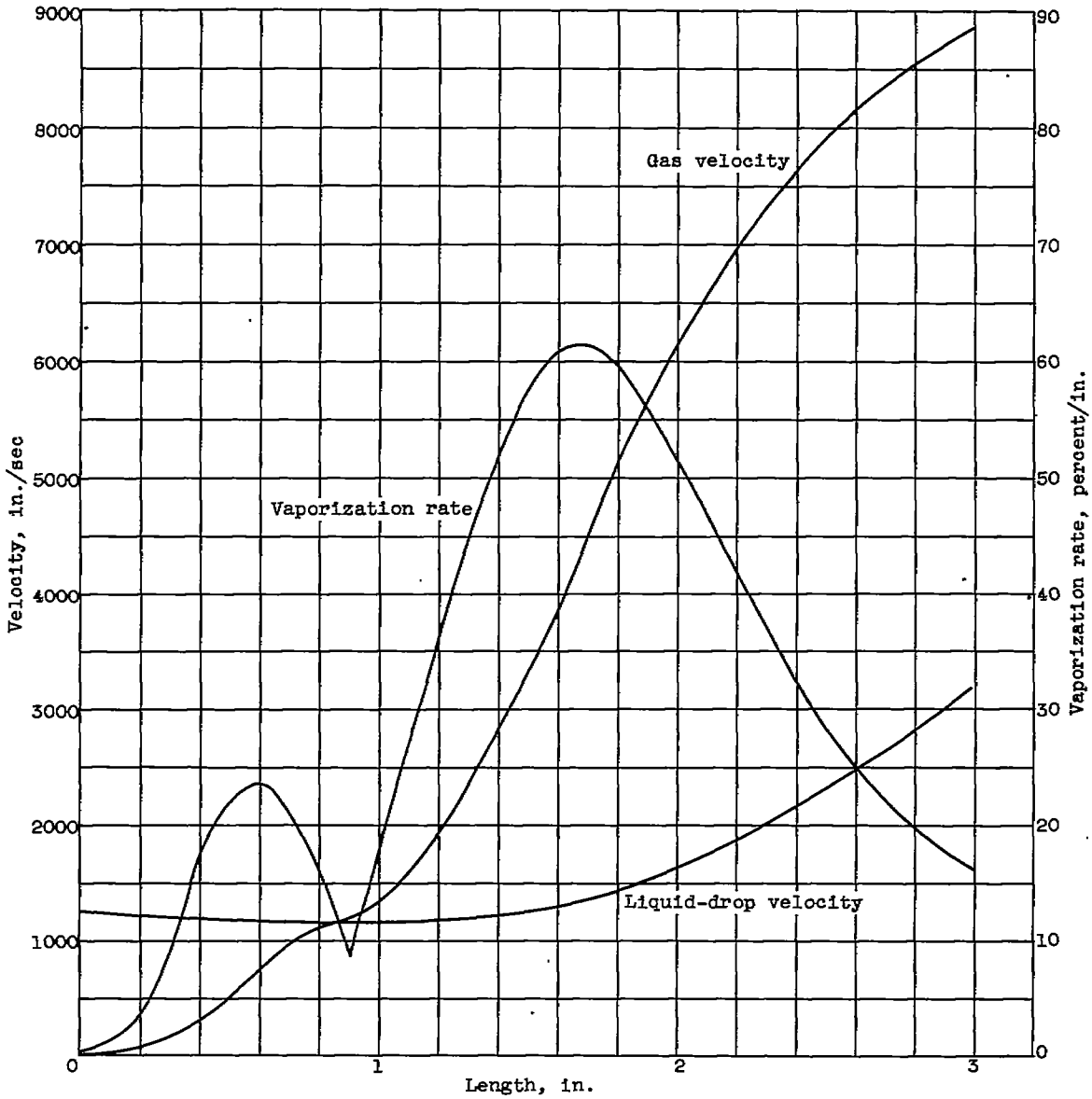

(b) Vaporization rate, and liquid-drop and gas velocity.

Figure 2. - Concluded. Typical droplet histories. Initial drop temperature, 500° R; initial drop velocity, 1200 inches per second; initial drop diameter, 0.006 inch (150 microns); final gas velocity, 9600 inches per second; chamber pressure, 300 pounds per square inch absolute; and chamber temperature, 5000° R.

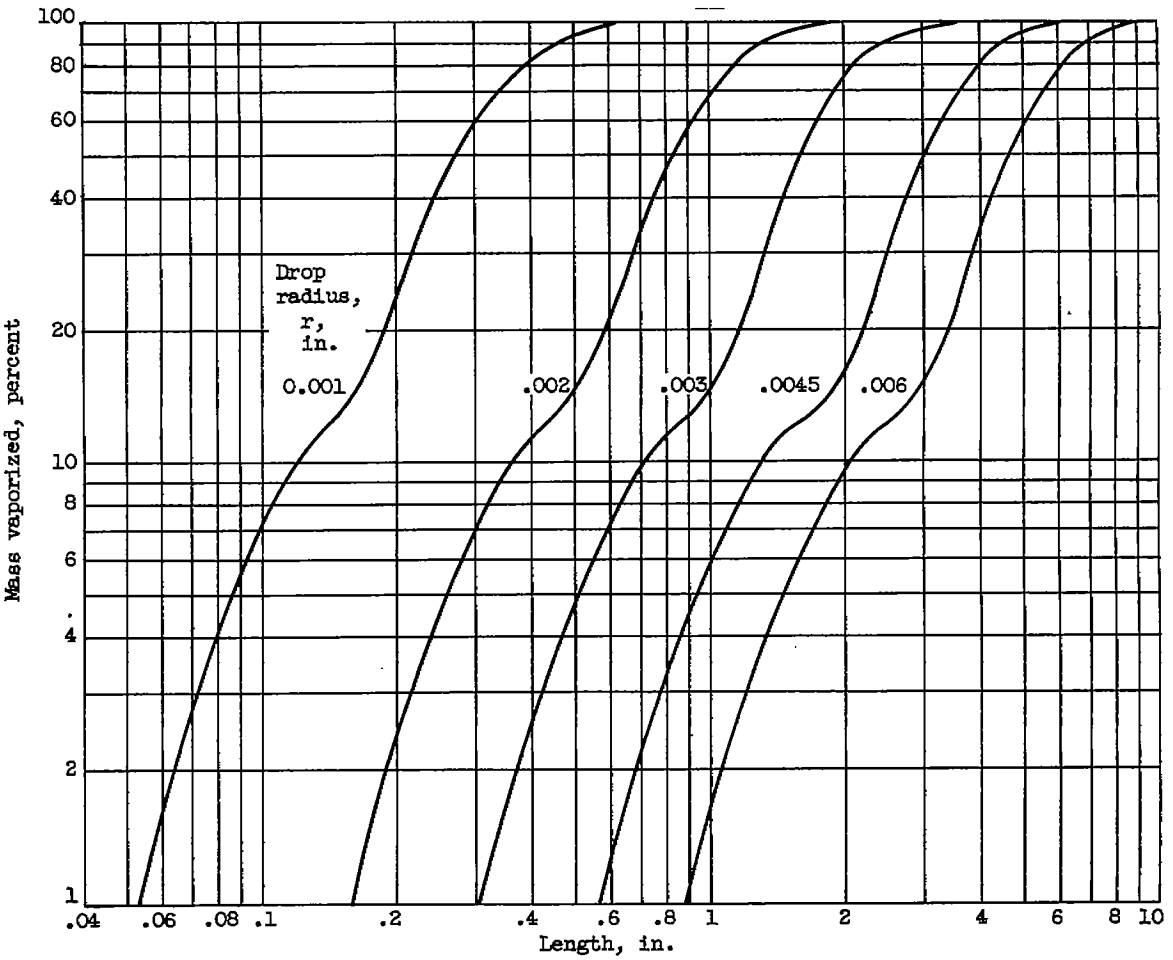

(a) Mass vaporized.

Figure 3. - Effect of drop size on vaporization. Initial drop temperature, 500° R; initial drop velocity, 1200 inches per second; final gas velocity, 9600 inches per second; chamber pressure, 300 pounds per square inch; and chamber temperature, 5000° R.

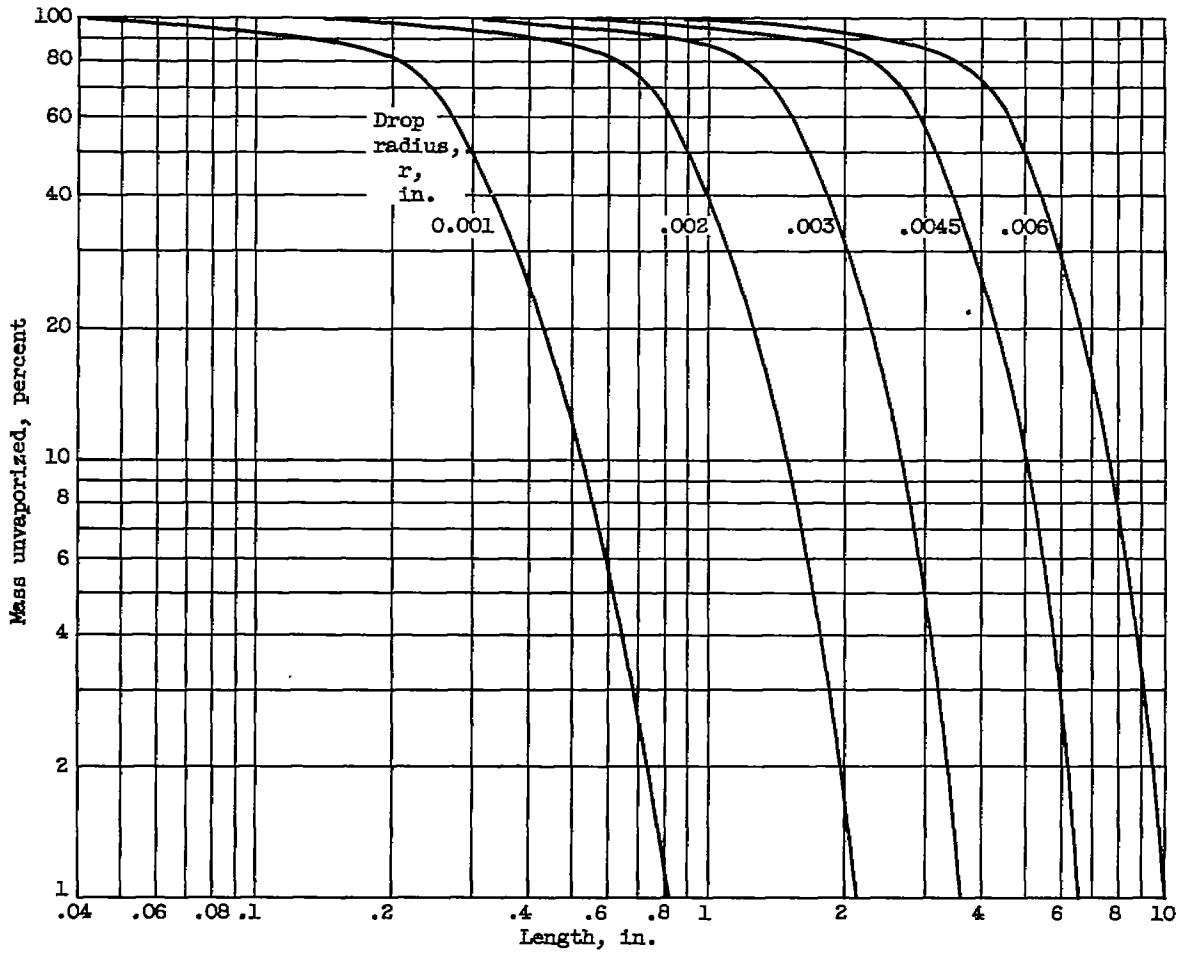

(b) Mass unvaporized.

Figure 3. - Continued. Effect of drop size on vaporization. Initial drop temperature, 500° R; initial drop velocity, 1200 inches per second; final gas velocity, 9600 inches per second; chamber pressure, 300 pounds per square inch; and chamber temperature, 5000° R.

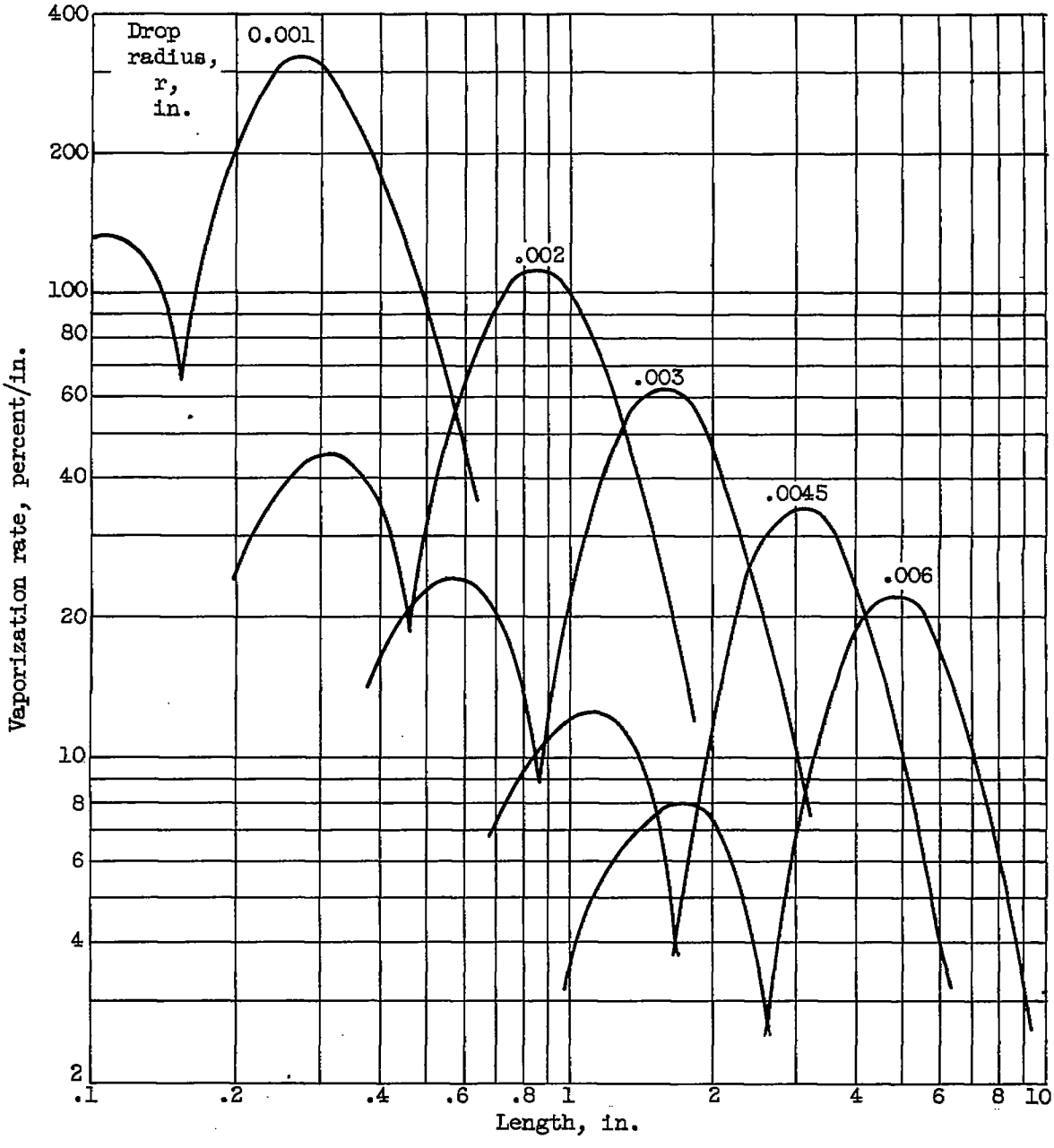

(c) Vaporization rate.

Figure 3. - Concluded. Effect of drop size on vaporization. Initial drop temperature, 500° R; initial drop velocity, 1200 inches per second; final gas velocity, 9600 inches per second; chamber pressure, 300 pounds per square inch; and chamber temperature, 5000° R.

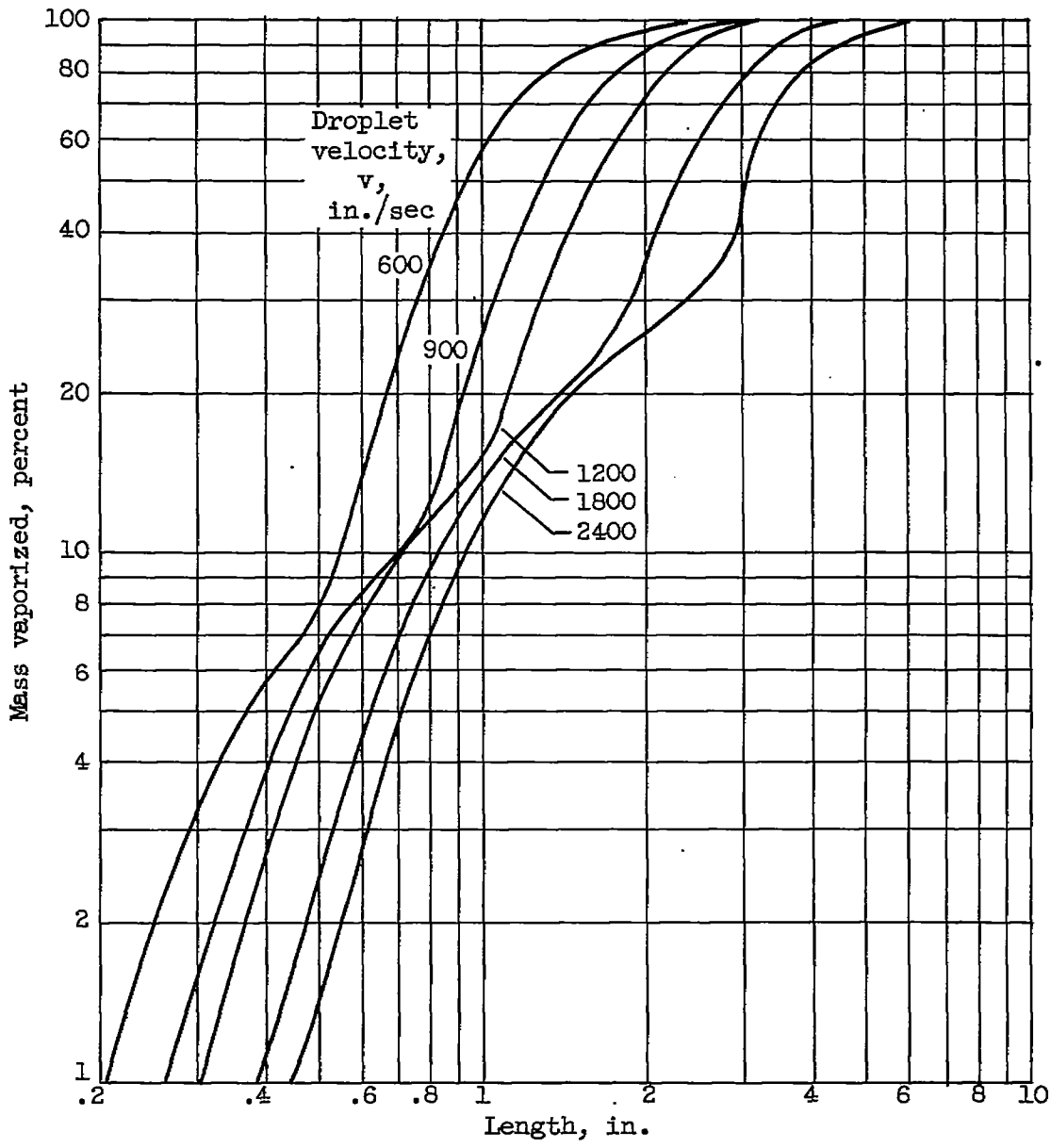

(a) Mass vaporized.

Figure 4. - Effect of initial drop velocity on vaporization. Initial drop diameter, 0.006 inch (150 microns); initial drop temperature, 500° R; final gas velocity, 9600 inches per second; chamber pressure, 300 pounds per square inch absolute; and chamber temperature, 5000° R.

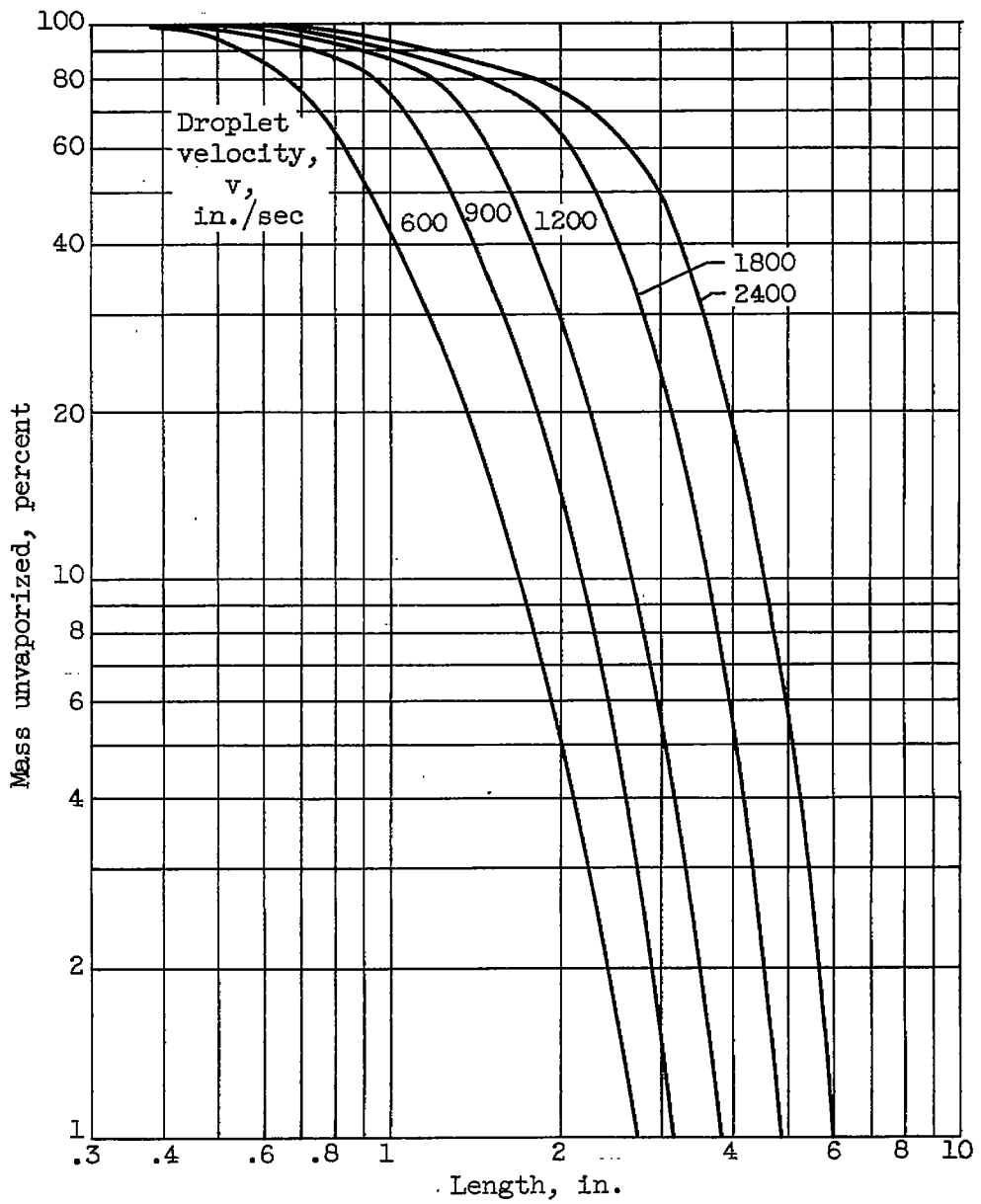

(b) Mass unvaporized.

Figure 4. - Continued. Effect of initial drop velocity on vaporization. Initial drop diameter, 0.006 inch (150 microns); initial drop temperature, 500° R; final gas velocity, 9600 inches per second; chamber pressure, 300 pounds per square inch absolute; and chamber temperature, 5000° R.

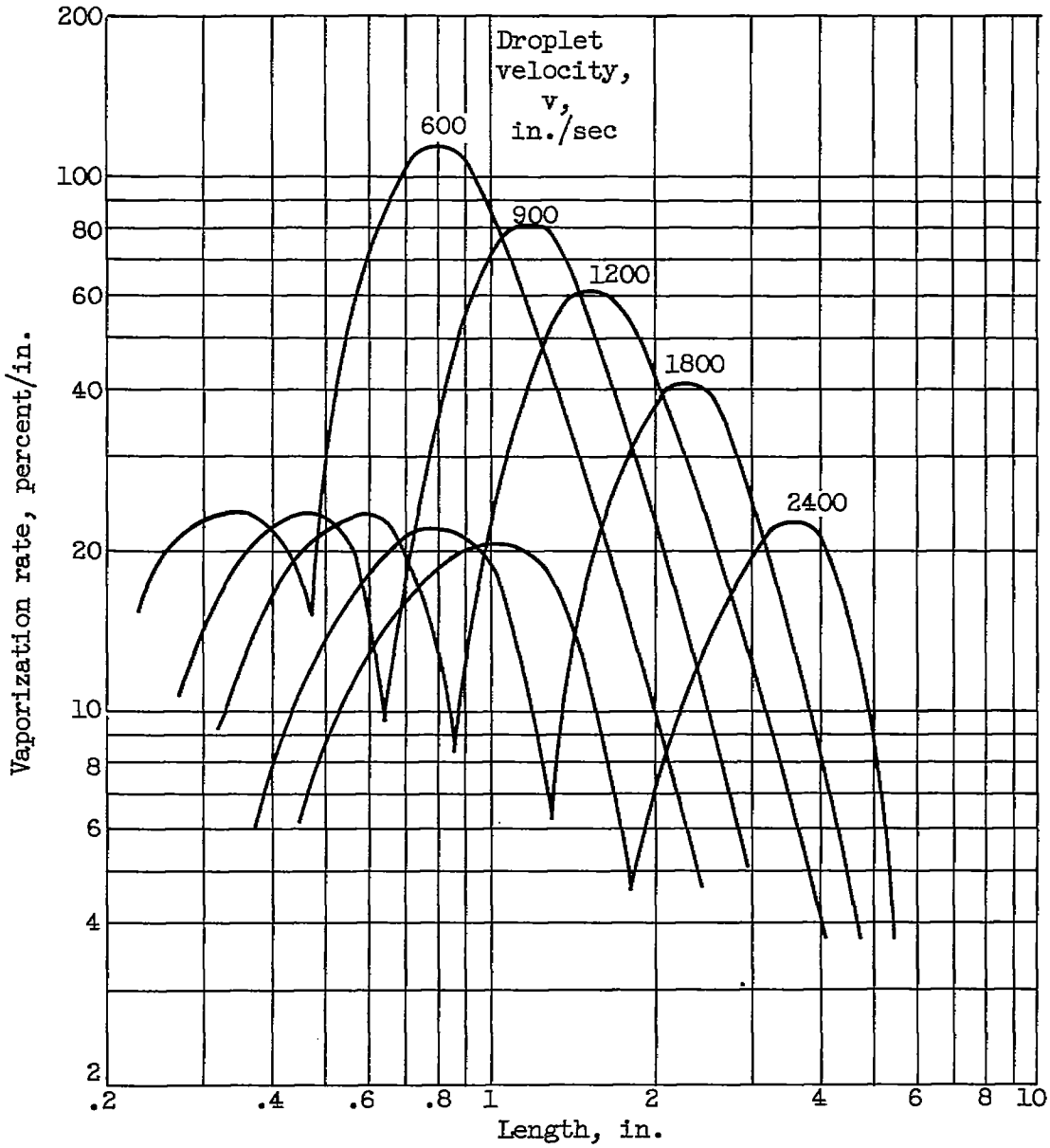

(c) Vaporization rate.

Figure 4. - Concluded. Effect of initial drop velocity on vaporization. Initial drop diameter, 0.006 inch (150 microns); initial drop temperature, 500° R; final gas velocity, 9600 inches per second; chamber pressure, 300 pounds per square inch absolute; and chamber temperature, 5000° R.

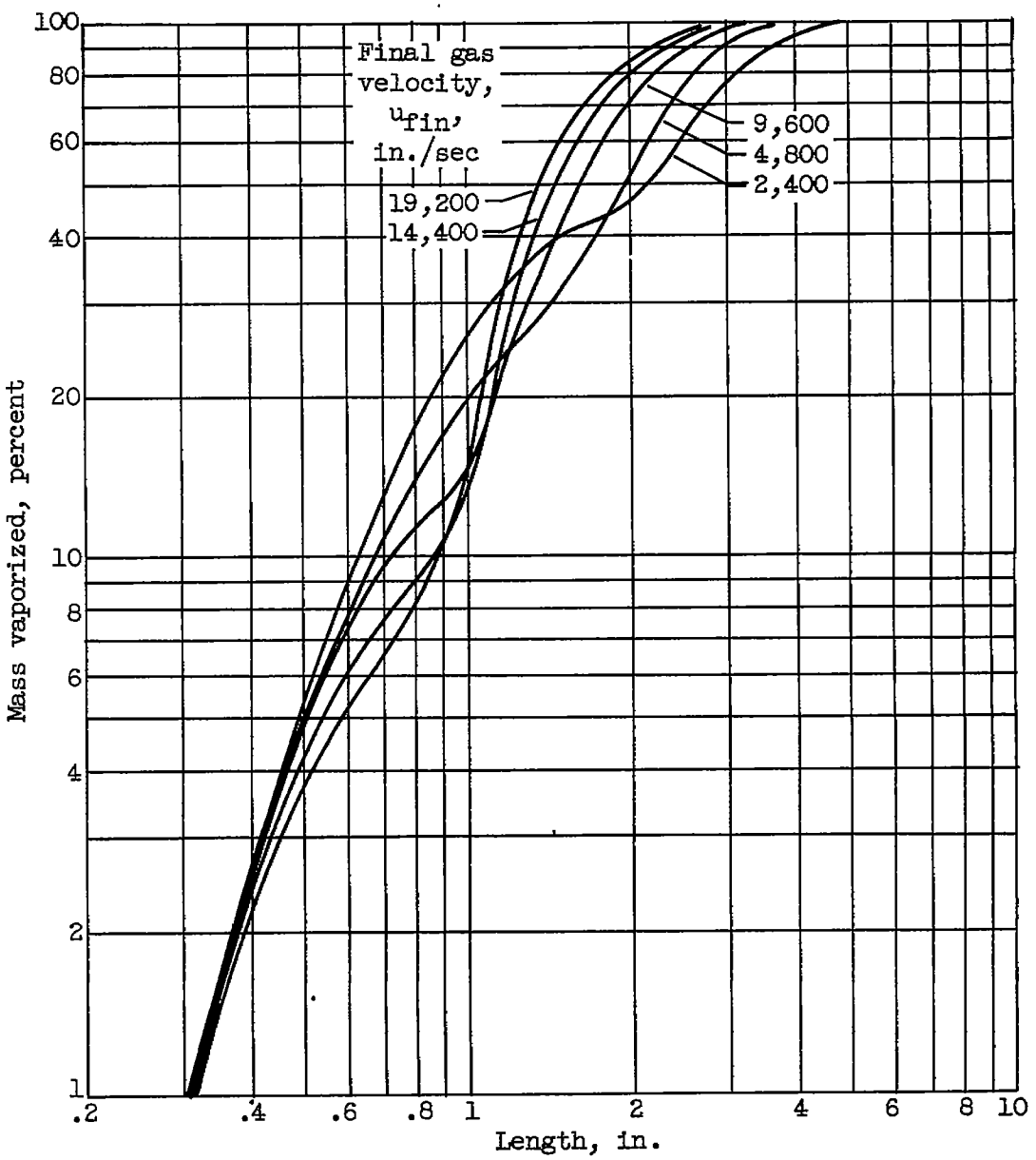

(a) Mass vaporized.

Figure 5. - Effect of final gas velocity on vaporization. Initial drop temperature, 500° R; initial drop velocity, 1200 inches per second; initial drop diameter, 0.006 inch (150 microns); chamber pressure, 300 pounds per square inch absolute; and chamber temperature, 5000° R.

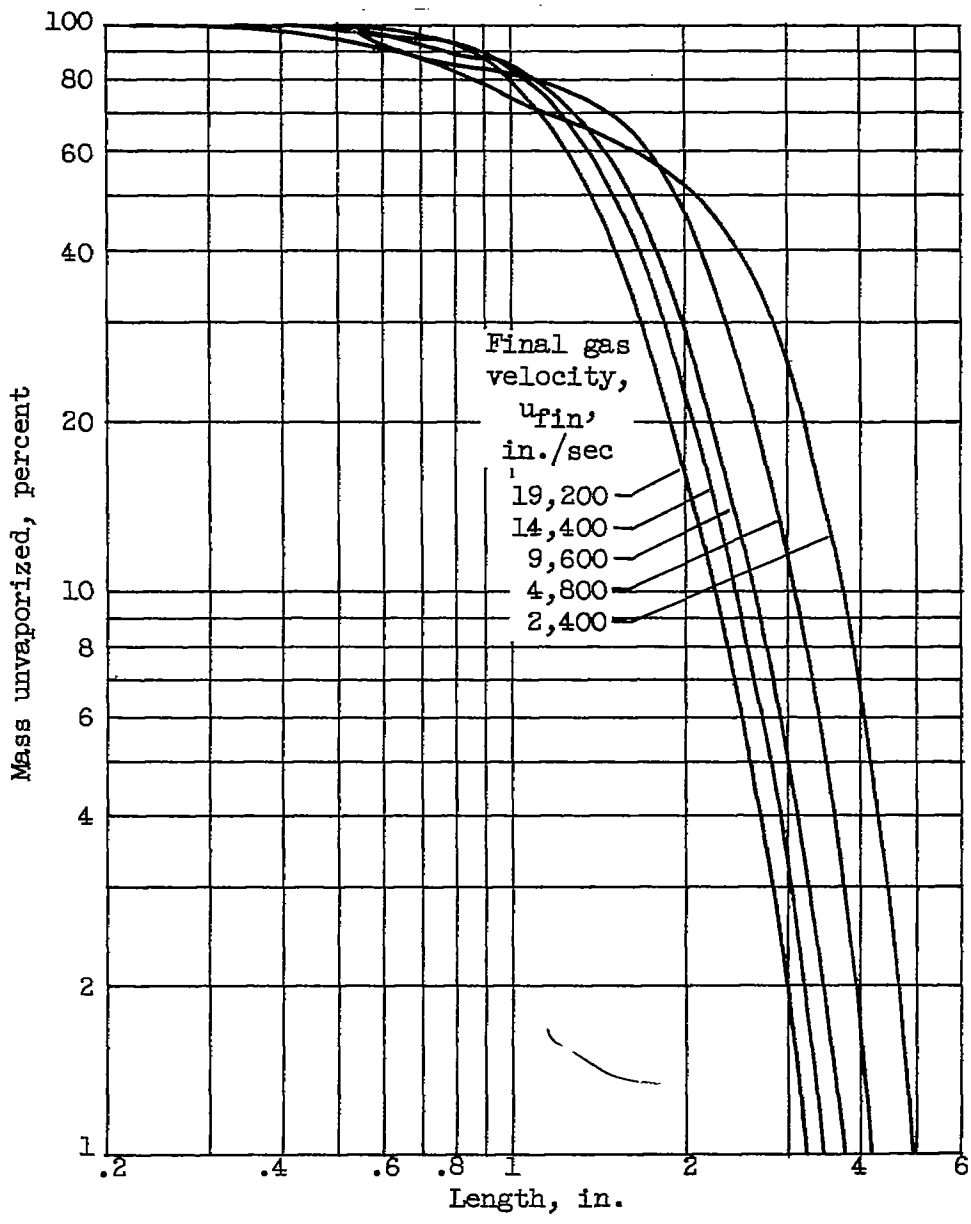

(b) Mass unvaporized.

Figure 5. - Continued. Effect of final gas velocity on vaporization. Initial drop temperature, 500° R; initial drop velocity, 1200 inches per second; initial drop diameter, 0.006 inch (150 microns); chamber pressure, 300 pounds per square inch absolute; and chamber temperature, 5000° R.

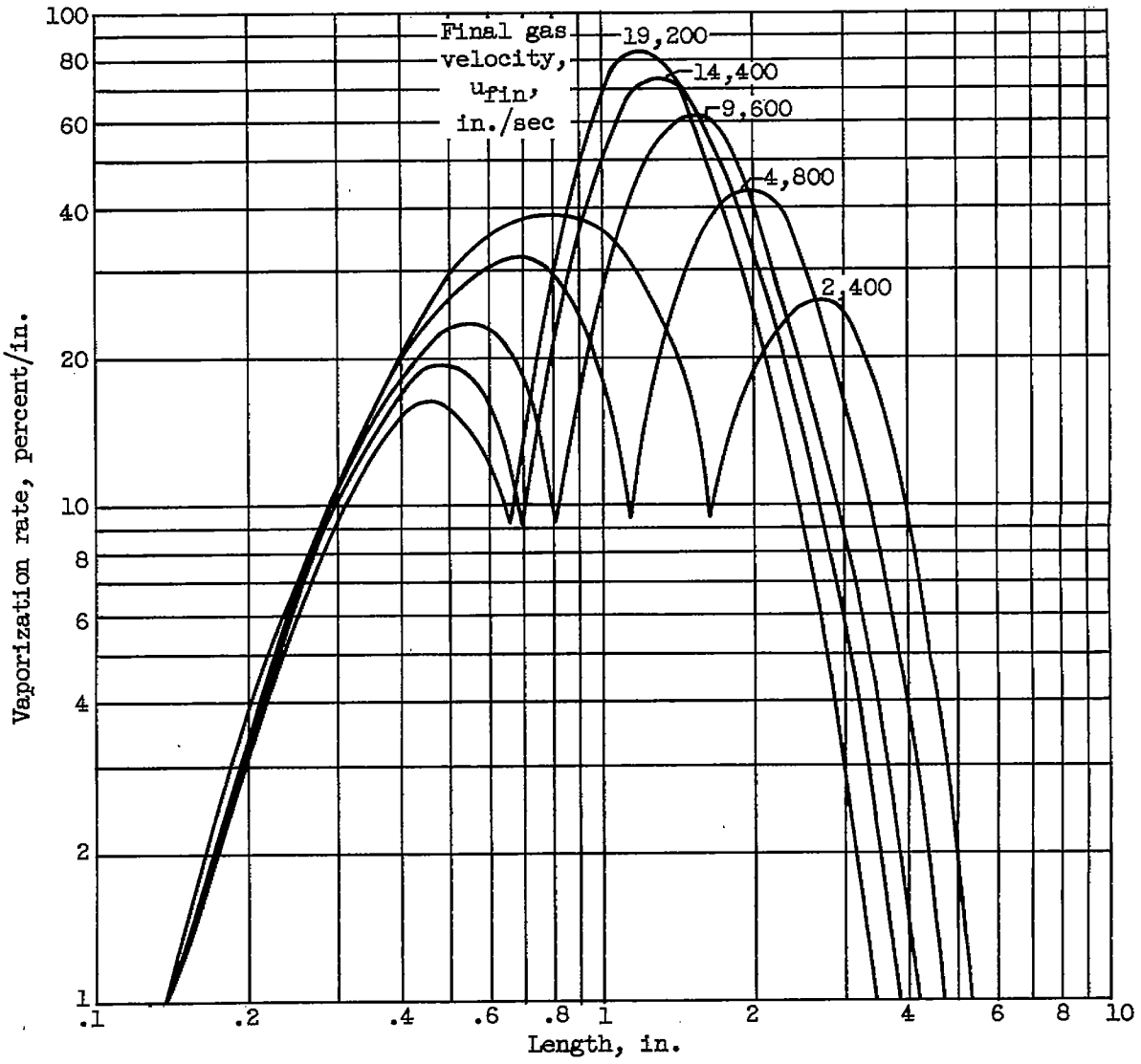

(c) Vaporization rate.

Figure 5. - Concluded. Effect of final gas velocity on vaporization. Initial drop temperature, 500° R; initial drop velocity, 1200 inches per second; initial drop diameter, 0.006 inch (150 microns); chamber pressure, 300 pounds per square inch absolute; and chamber temperature, 5000° R.

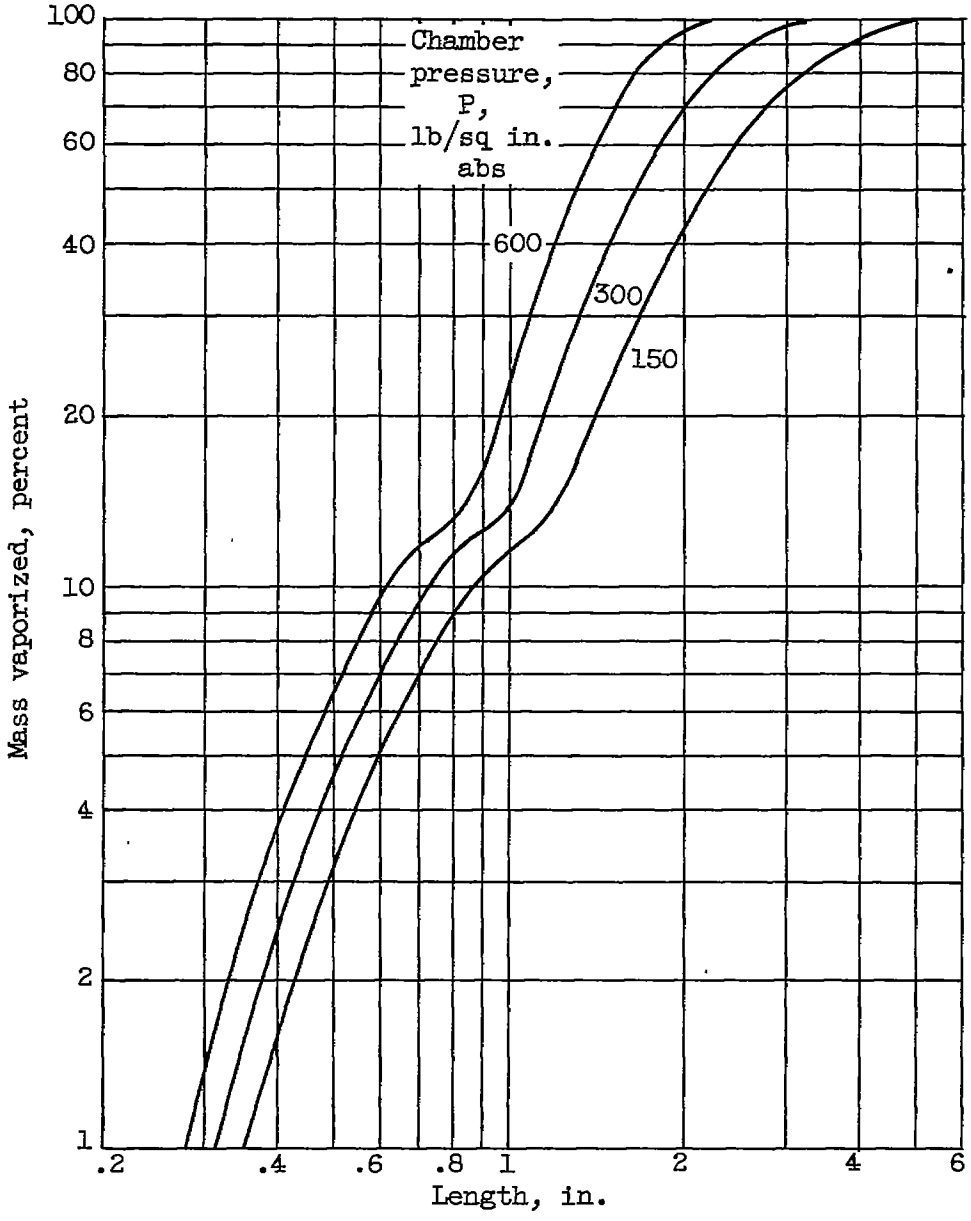

(a) Mass vaporized.

Figure 6. - Effect of chamber pressure on vaporization. Initial drop temperature, 500° R; initial drop velocity, 1200 inches per second; initial drop diameter, 0.006 inch (150 microns); final gas velocity, 9600 inches per second; and chamber temperature, 5000° R.

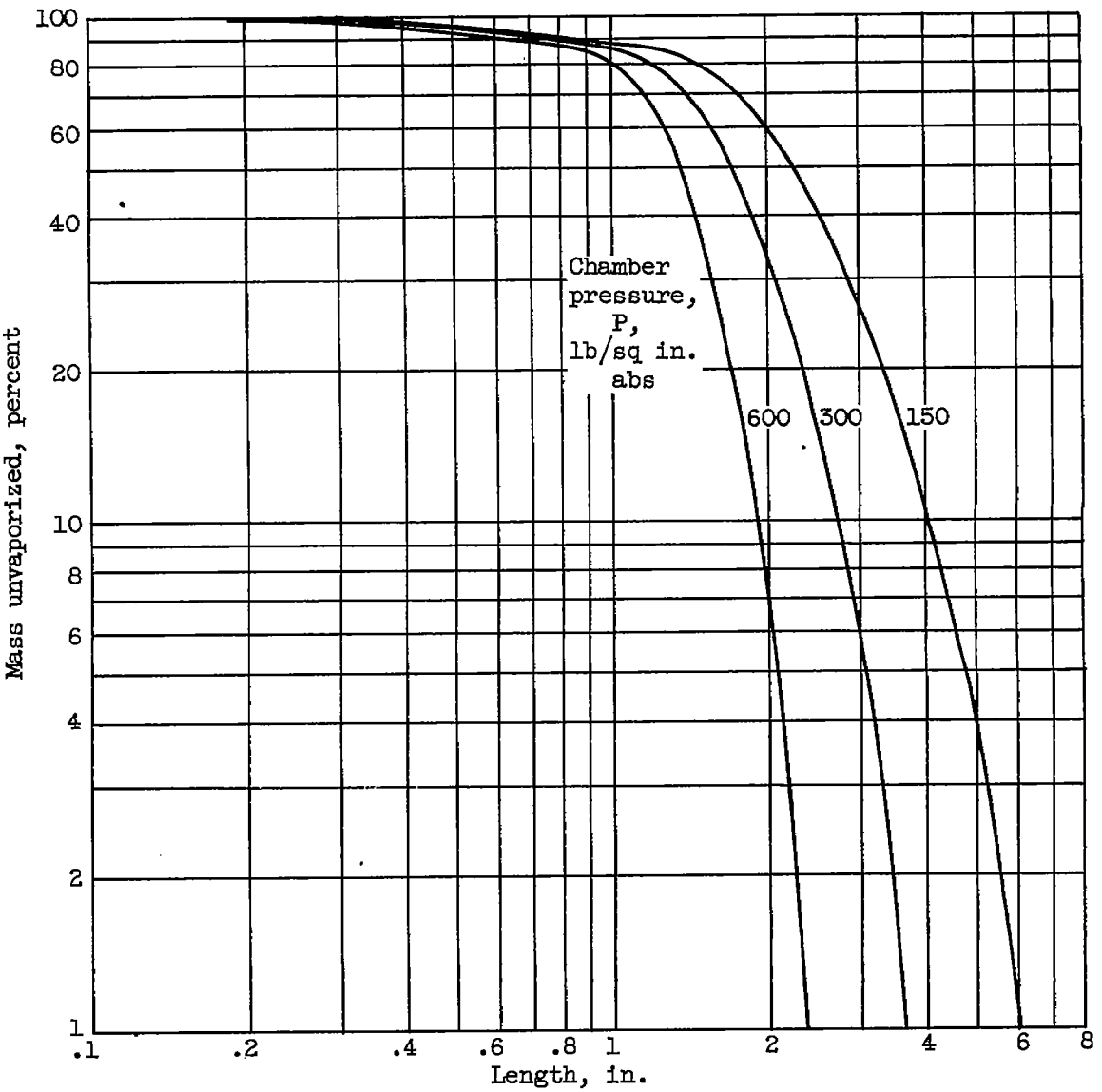

(b) Mass unvaporized.

Figure 6. - Continued. Effect of chamber pressure on vaporization. Initial drop temperature, 500° R; initial drop velocity, 1200 inches per second; initial drop diameter, 0.006 inch (150 microns); final gas velocity, 9600 inches per second; and chamber temperature, 5000° R.

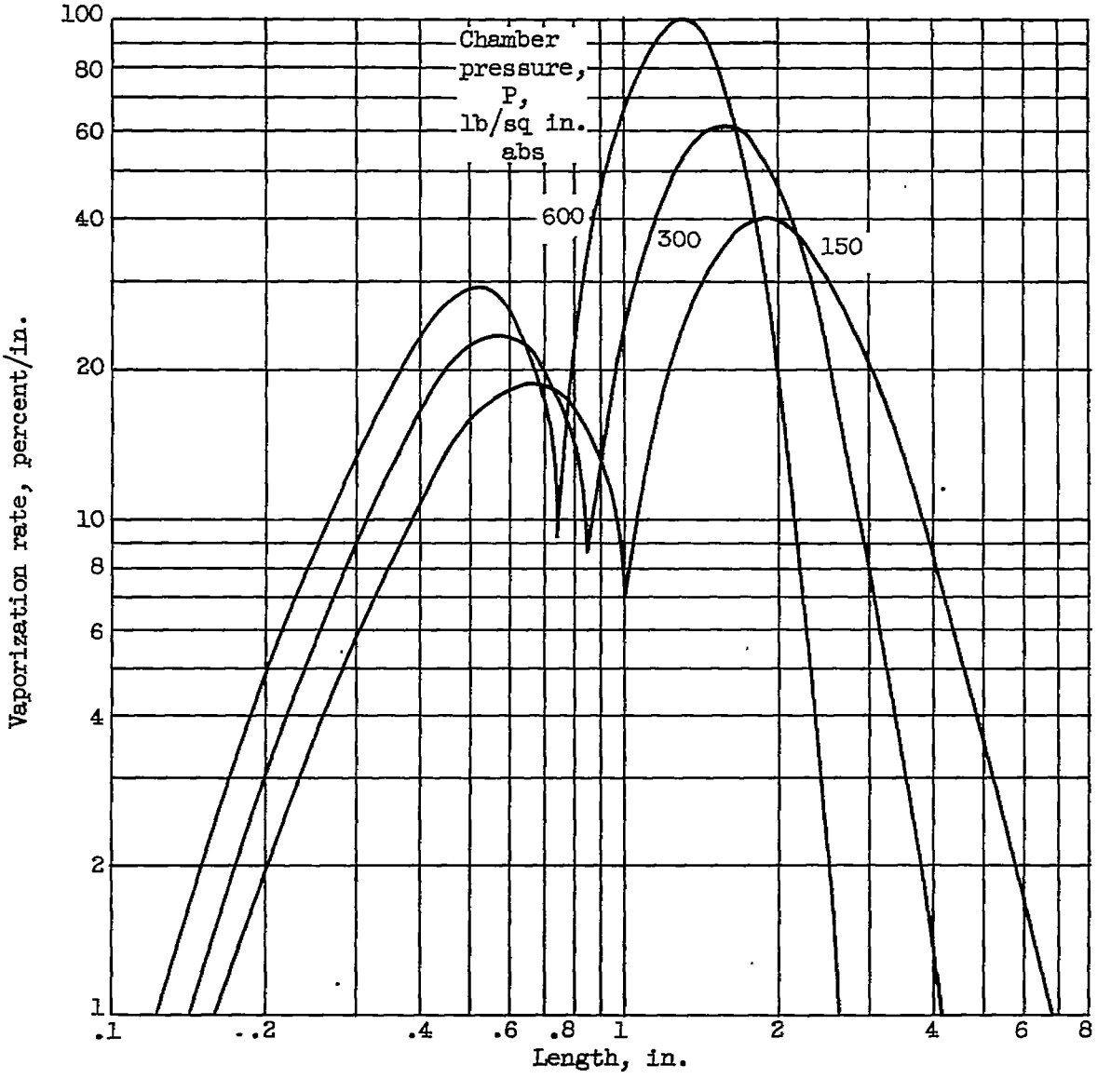

(c) Vaporization rate.

Figure 6. - Concluded. Effect of chamber pressure on vaporization. Initial drop temperature, 500° R; initial drop velocity, 1200 inches per second; initial drop diameter, 0.006 inch (150 microns); final gas velocity, 9600 inches per second; and chamber temperature, 5000° R.

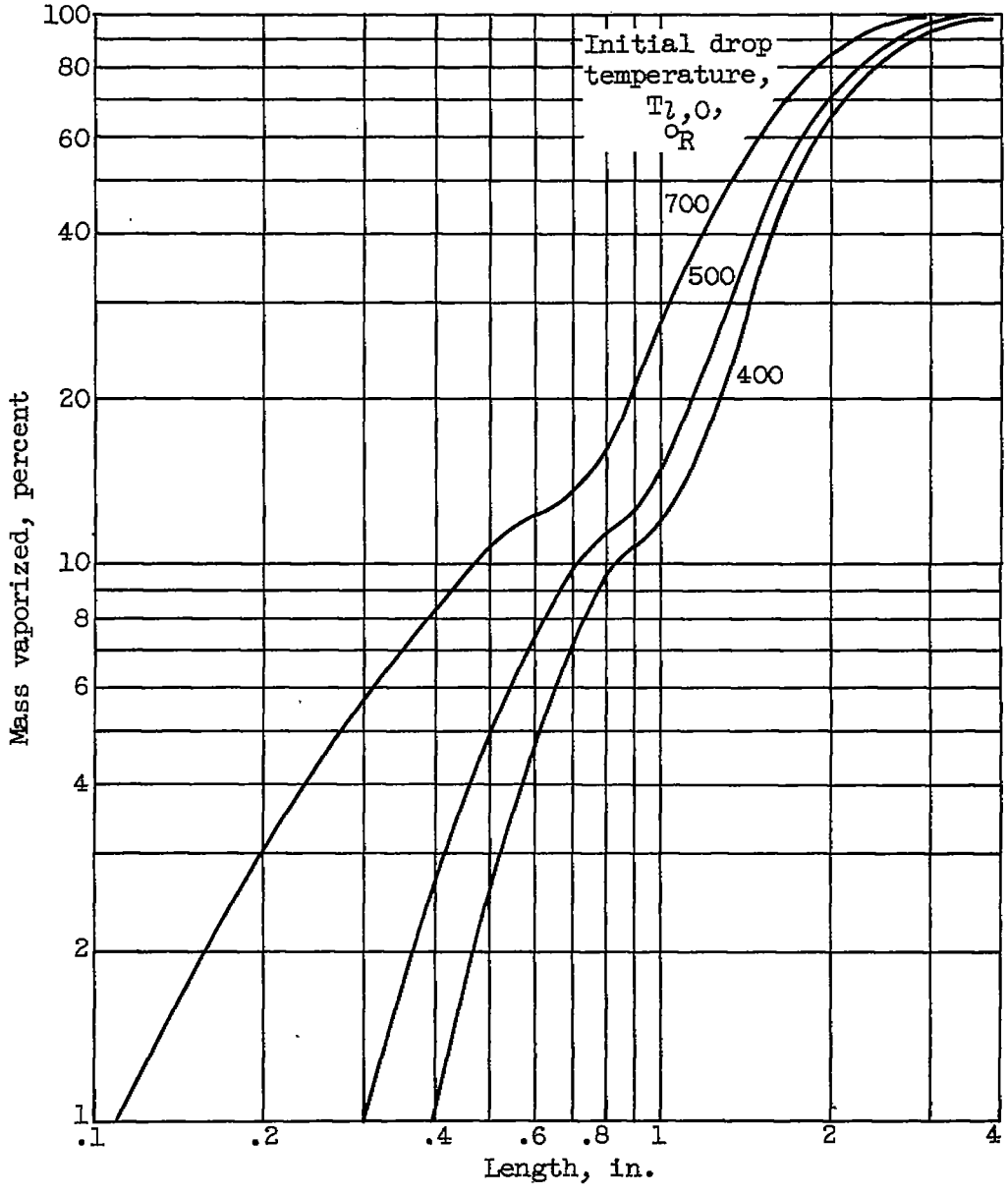

(a) Mass vaporized.

Figure 7. - Effect of initial liquid temperature on vaporization. Initial drop velocity, 1200 inches per second; initial drop diameter, 0.006 inch (150 microns); final gas velocity, 9600 inches per second; chamber pressure, 300 pounds per square inch absolute; and chamber temperature, 5000° R.

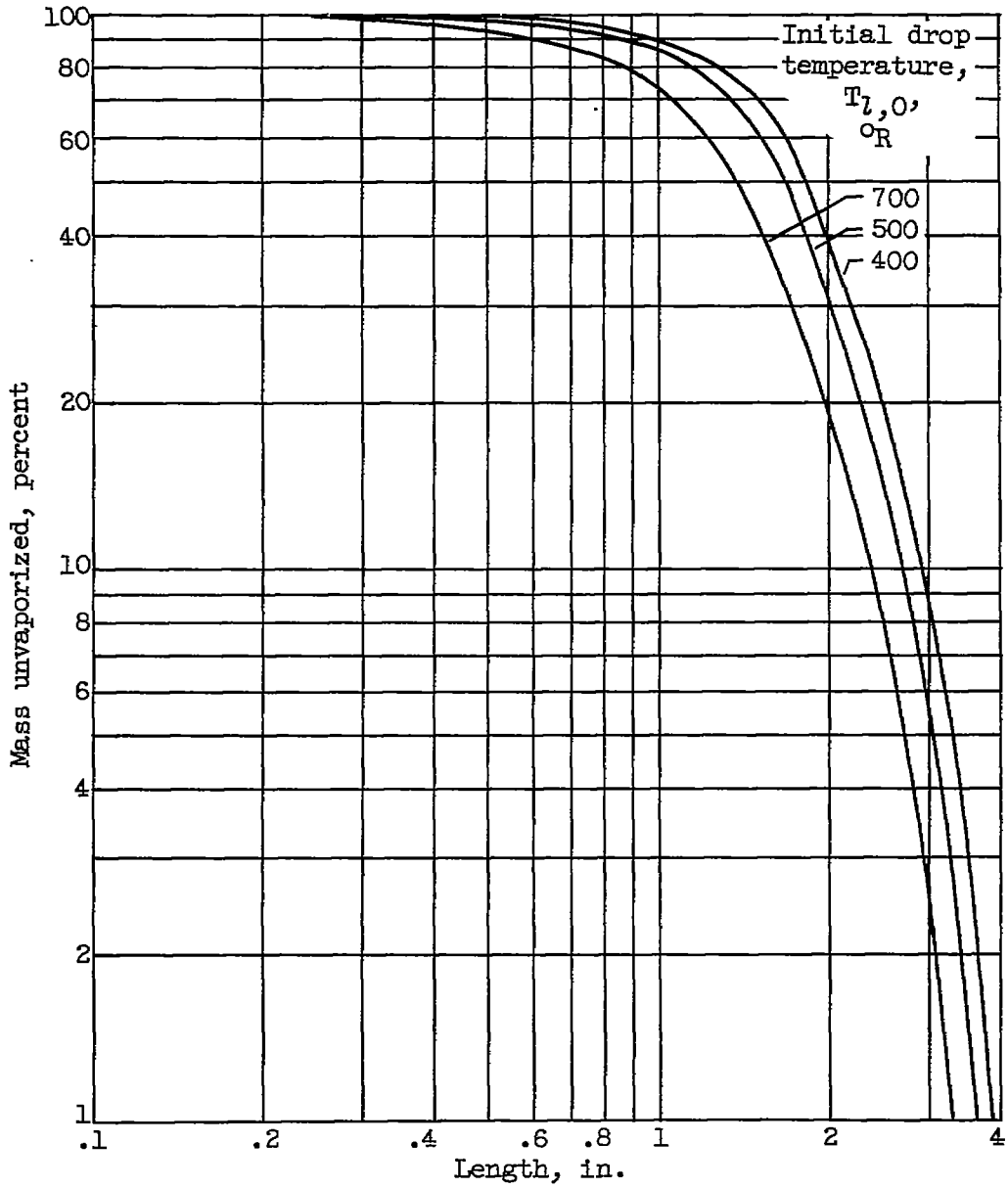

(b) Mass unvaporized.

Figure 7. - Continued. Effect of initial liquid temperature on vaporization. Initial drop velocity, 1200 inches per second; initial drop diameter, 0.006 inch (150 microns); final gas velocity, 9600 inches per second; chamber pressure, 300 pounds per square inch absolute; and chamber temperature, 5000° R.

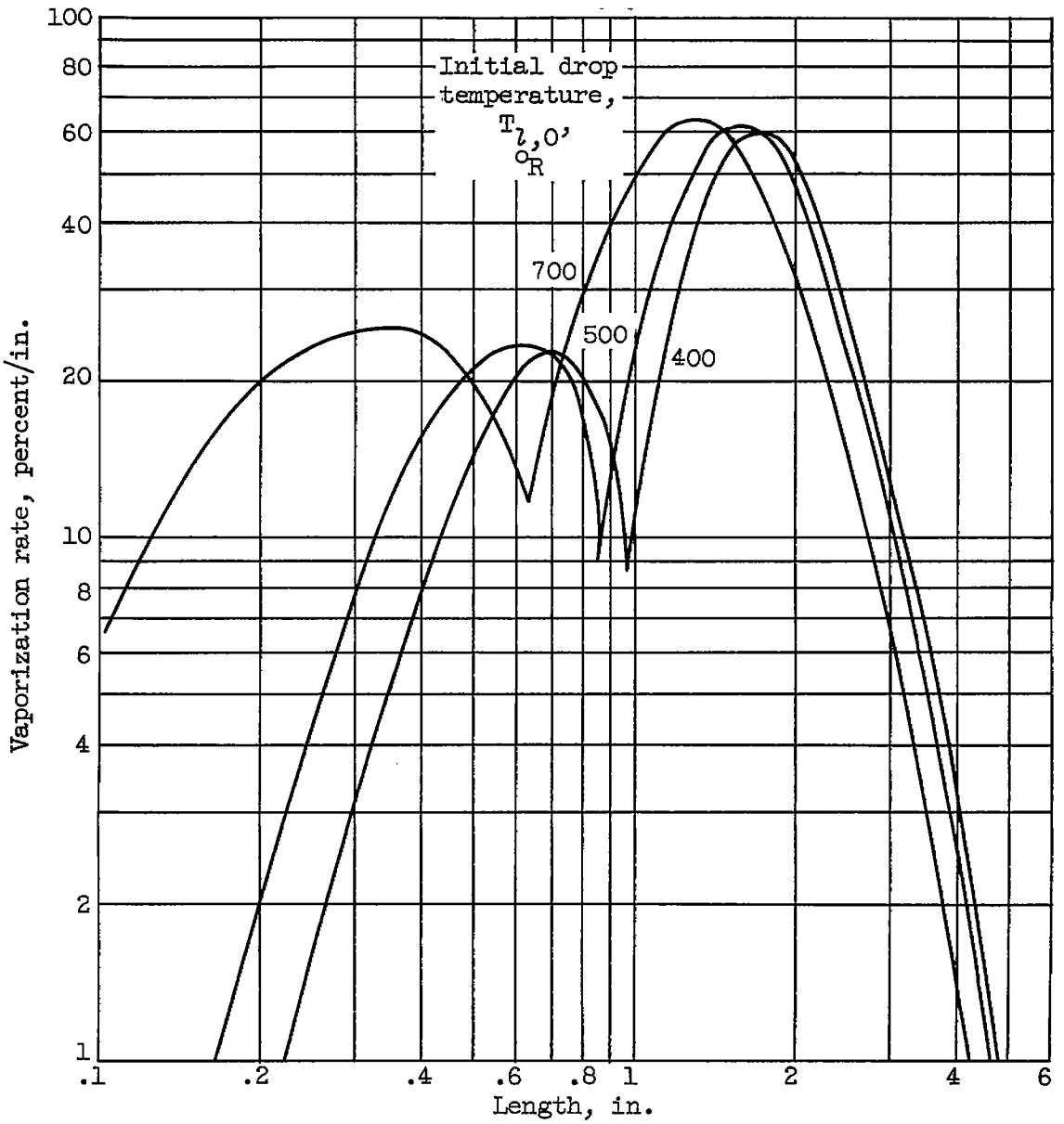

(c) Vaporization rate.

Figure 7. - Concluded. Effect of initial liquid temperature on vaporization. Initial drop velocity, 1200 inches per second; initial drop diameter, 0.006 inch (150 microns); final gas velocity, 9600 inches per second; chamber pressure, 300 pounds per square inch absolute; and chamber temperature, 5000° R.

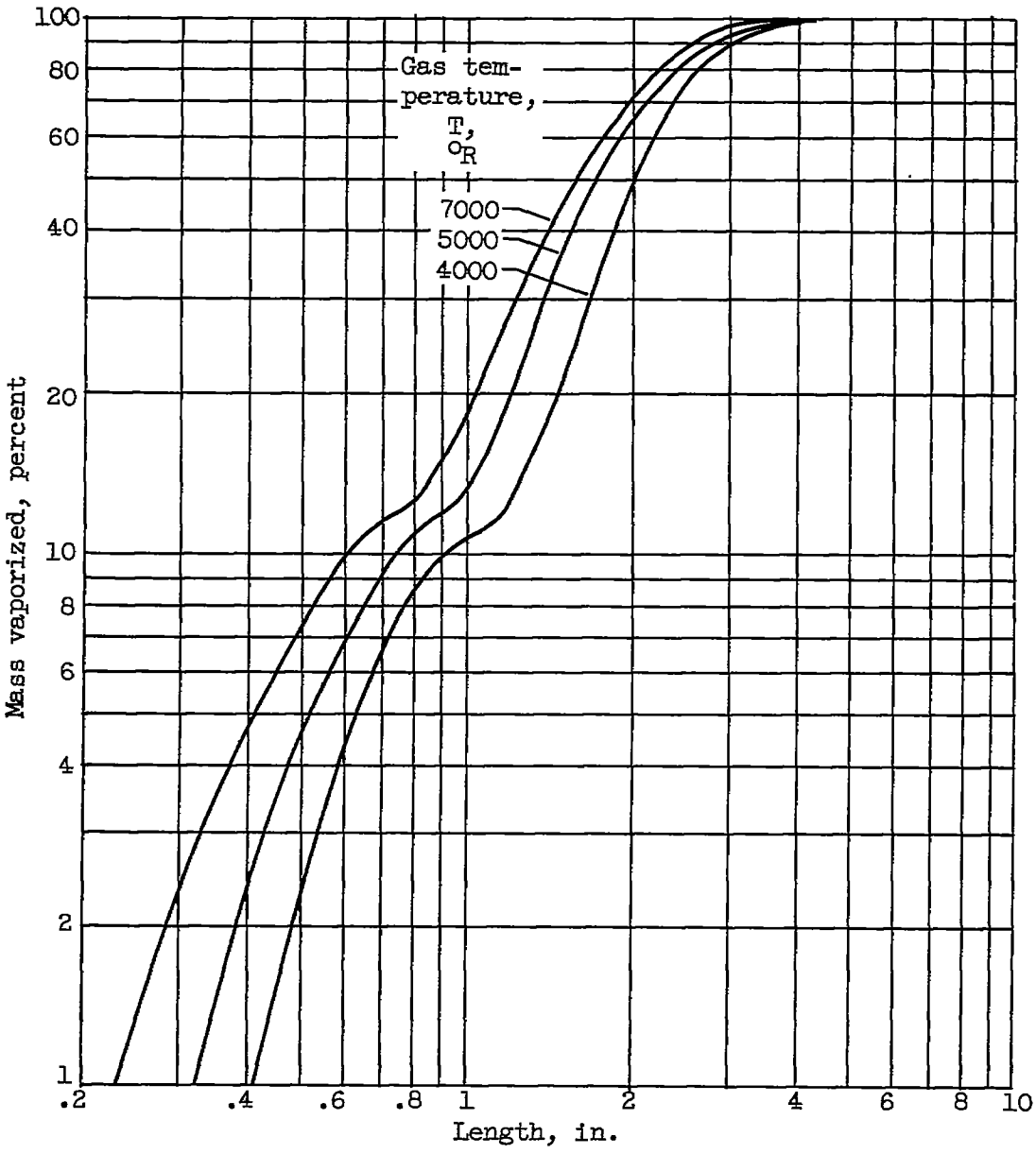

(a) Mass vaporized.

Figure 8. - Effect of gas temperature on vaporization. Initial drop temperature, 500° R; initial drop velocity, 1200 inches per second; initial drop diameter, 0.006 inch (150 microns); final gas velocity, 9600 inches per second; and chamber pressure, 300 pounds per square inch absolute.

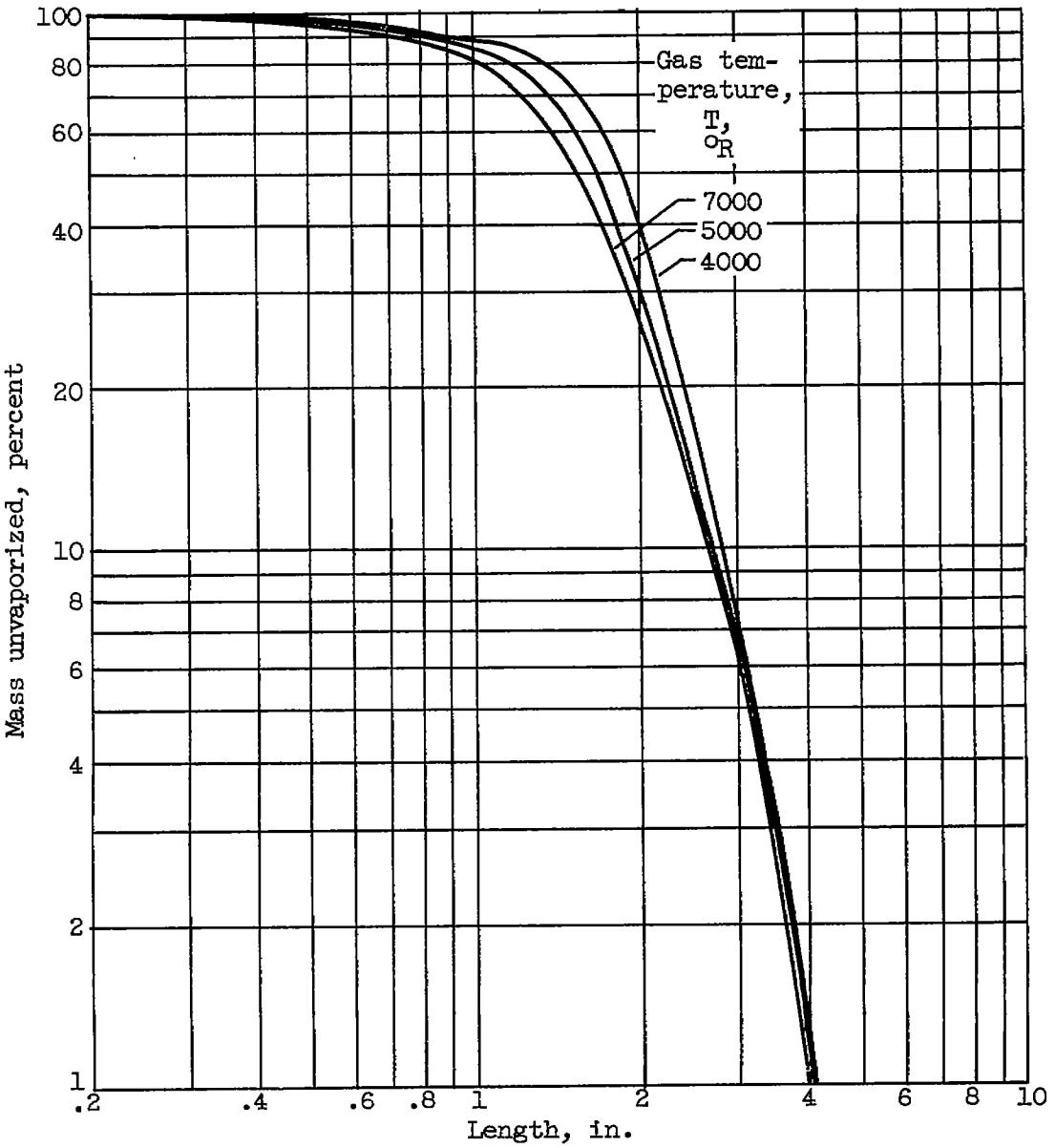

(b) Mass unvaporized.

Figure 8. - Continued. Effect of gas temperature on vaporization. Initial drop temperature, 500° R; initial drop velocity, 1200 inches per second; initial drop diameter, 0.006 inch (150 microns); final gas velocity, 9600 inches per second; and chamber pressure, 300 pounds per square inch absolute.

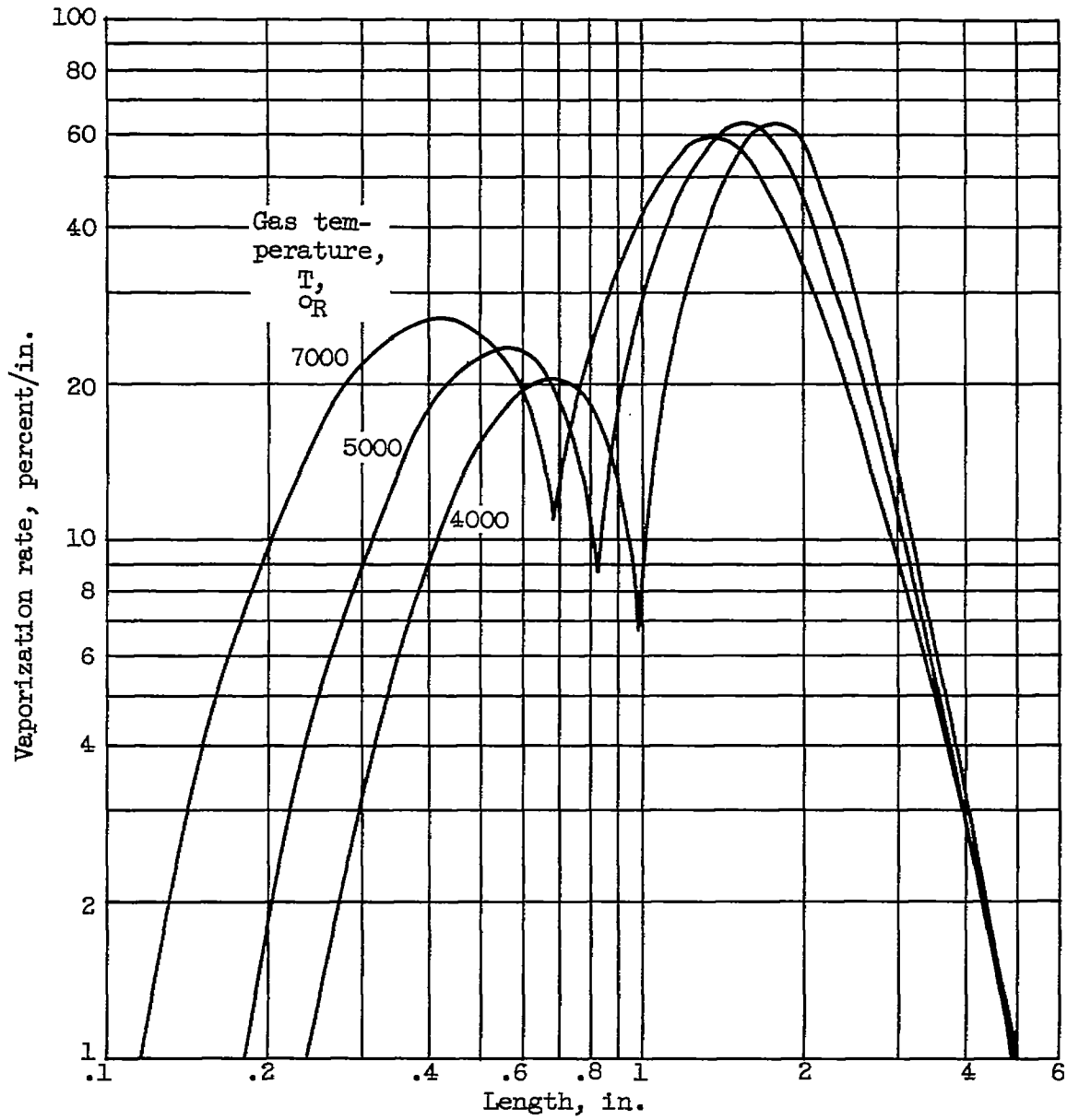

(c) Vaporization rate.

Figure 8. - Concluded. Effect of gas temperature on vaporization. Initial drop temperature, 500° R; initial drop velocity, 1200 inches per second; initial drop diameter, 0.006 inch (150 microns); final gas velocity, 9600 inches per second; and chamber pressure, 300 pounds per square inch absolute.

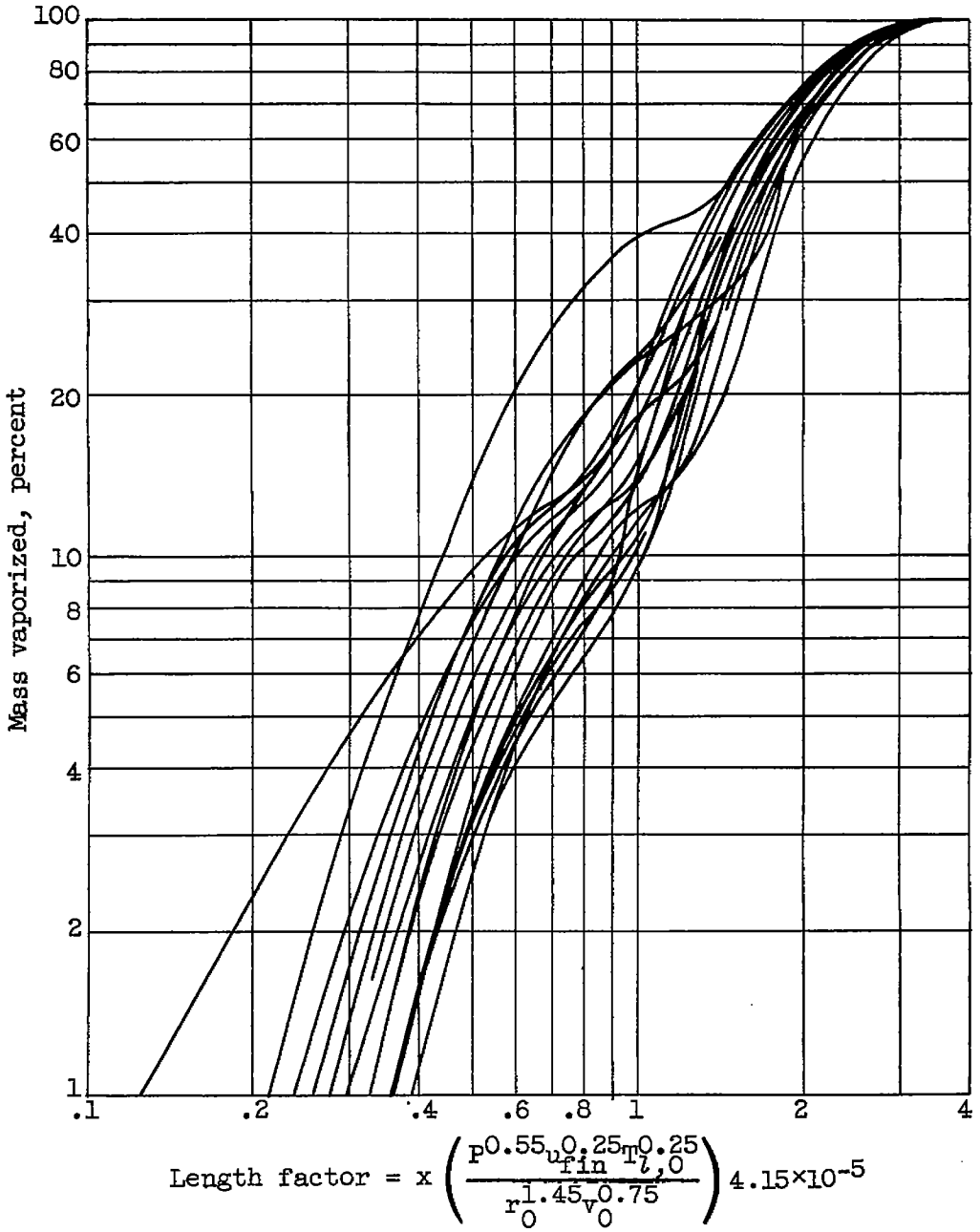

(a) Mass vaporized.

Figure 9. - Correlation of results.

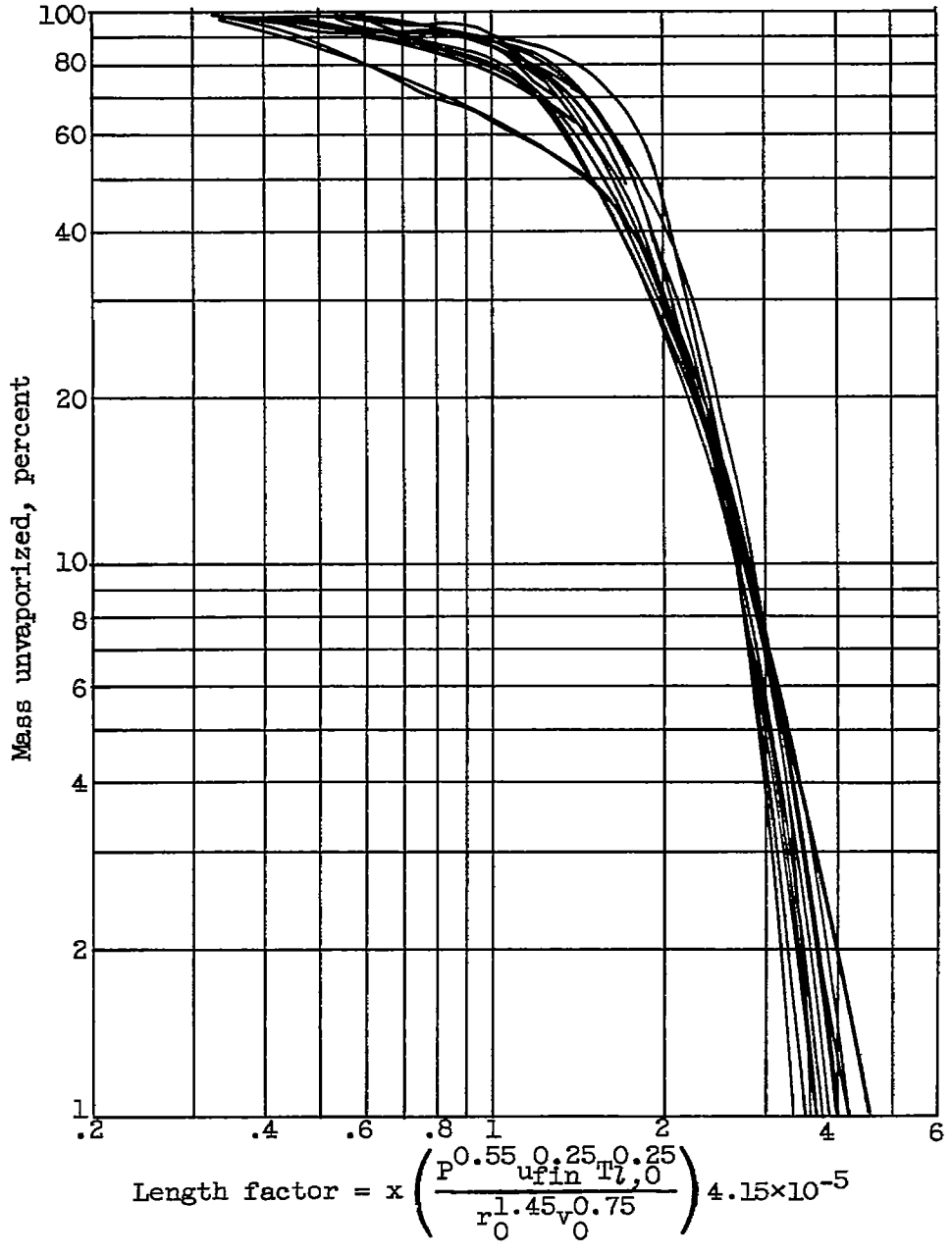

(b) Mass unvaporized.

Figure 9. - Concluded. Correlation of results.

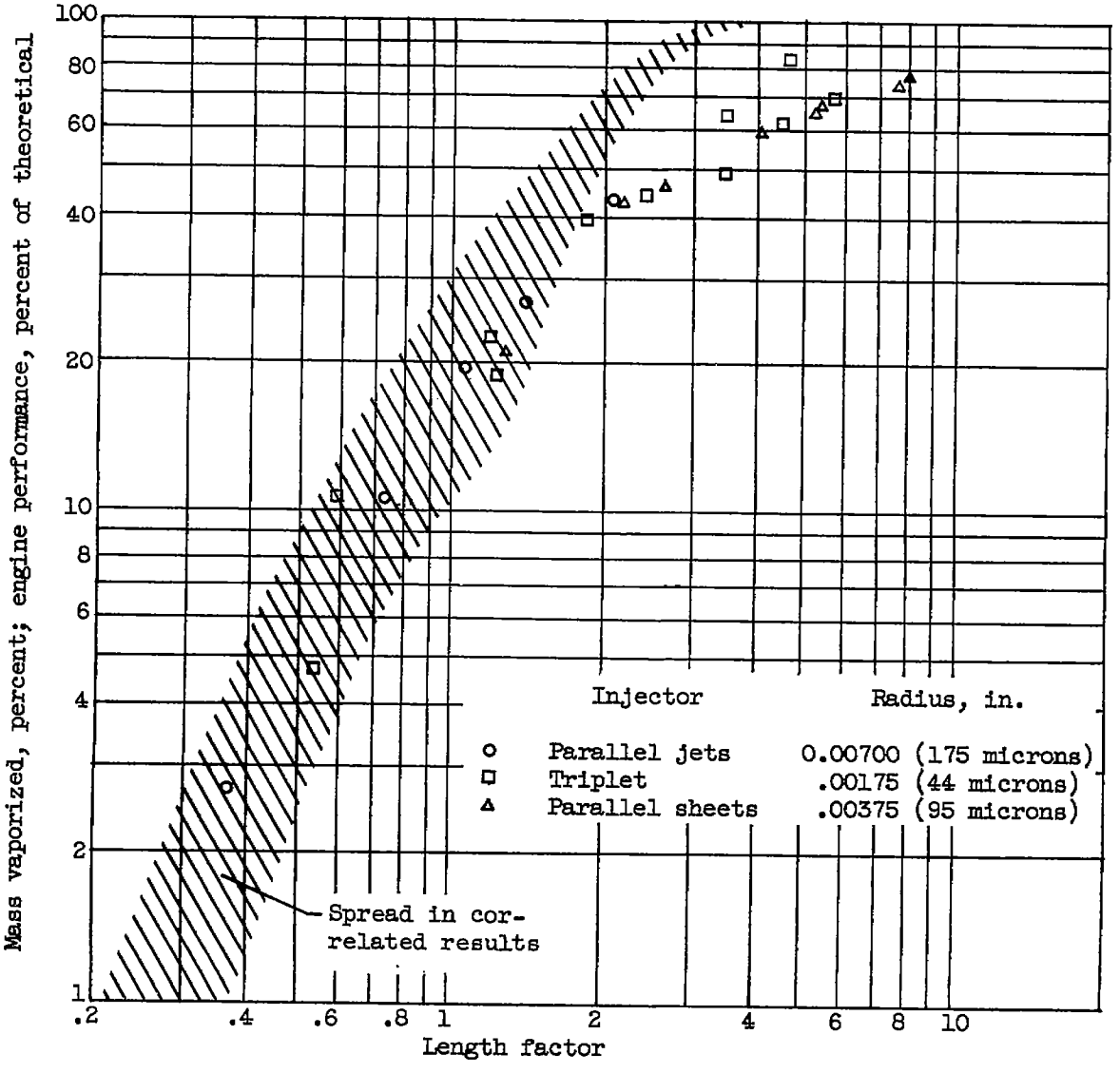

(a) Mass vaporized.

Figure 10. - Comparison of experimental and calculated results. Initial temperature, 520° R; initial velocity, 600 inches per second; final gas velocity, 4800 inches per second; chamber pressure, 250 pounds per square inch; and chamber temperature, 5000° R.

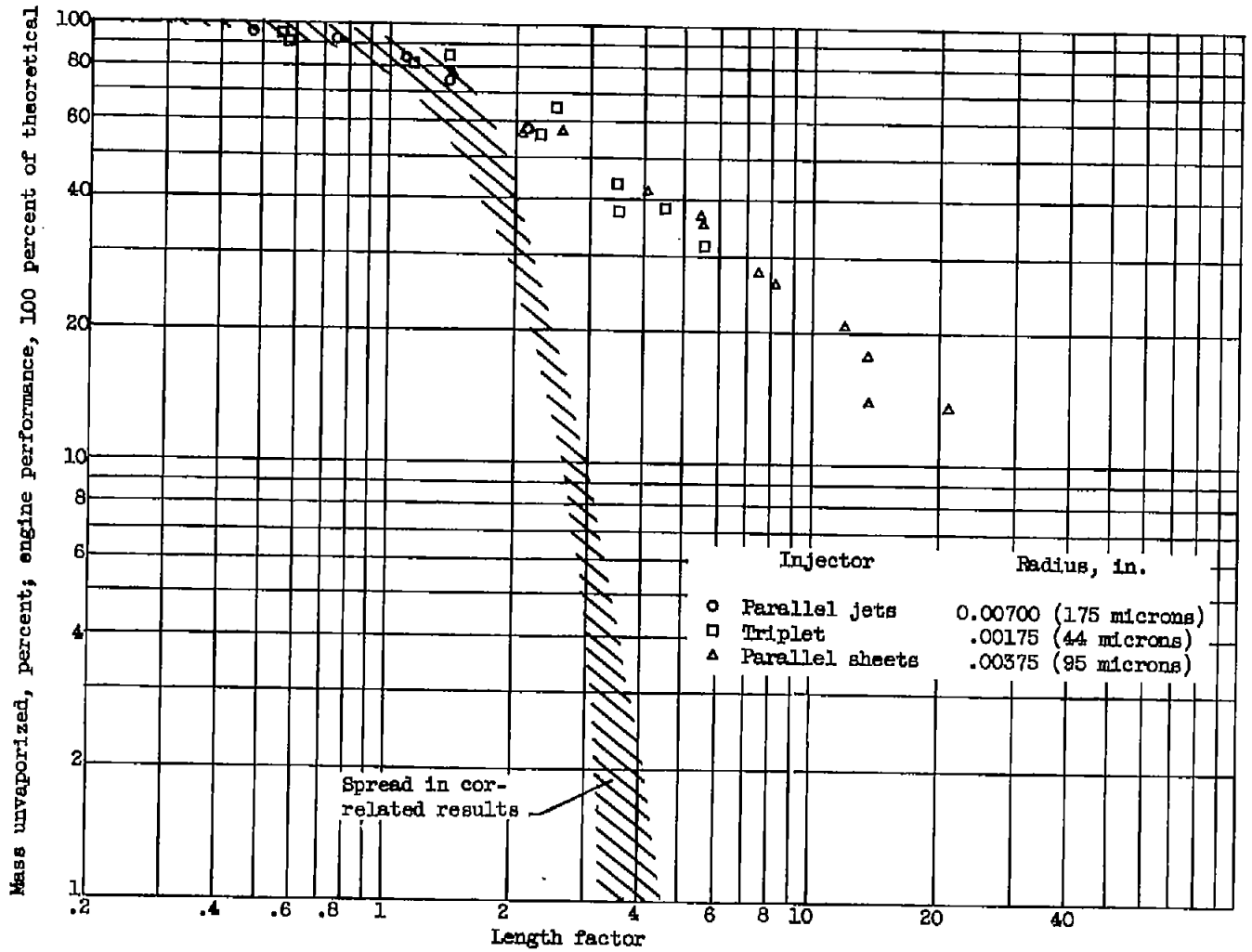

(b) Mass unvaporized.

Figure 10. - Concluded. Comparison of experimental and calculated results. Initial temperature, 520° R; initial velocity, 600 inches per second; final gas velocity, 4800 inches per second; chamber pressure, 250 pounds per square inch; and chamber temperature, 5000° R.